

GSI Annual Report 2003 (extracts)

Chemistry

Indication for a gaseous element 112 *Page 3*

S. Soverna

Theoretical predictions of the adsorption energy of element 112 on a gold surface *Page 4*

C. Sarpe-Tudoran, V. Pershina, B. Fricke, J. Anton, W.-D. Sepp

Empirical Relation between the Adsorption Properties on Gold Surfaces and Volatility of the Elements 112 and 114. *Page 5*

R. Eichler

Relativistic Effects on the Electronic Structure and Volatility of Group-8 tetroxides MO_4 , where M = Ru, Os and Element 108, Hs *Page 6*

V. Pershina, T. Bastug, B. Fricke

Predictions of Adsorption Temperature for the Heaviest Elements and a Measure of Volatility *Page 7*

V. Pershina

Final result of the CALLISTO-experiment: Formation of sodium hassate(VIII) *Page 8*

A. von Zweidorf, R. Angert, W. Bröchle, S. Bürger, K. Eberhardt, R. Eichler, H. Hummrich, E. Jäger, R. Jera, H.-O. Kling, J.V. Kratz, U. Krille, B. Kuczewski, G. Langrock, G. Lehr, M. Mendel, A. Nähler, A. Peil, V. Pershina, U. Rieth, M. Schädel, B. Schausten, E. Schimpf, H.-J. Schött, E. Stiel, P. Thörle, N. Trautmann, K. Tsukada, N. Wiehl, G. Wirth

Approaching first experiments with element 114 *Page 9*

A. Yakushev, W. Bröchle, E. Jäger, E. Schimpf, M. Schädel, A. Türler, B. Wierczinski

Gas chromatography of short-lived Hg isotopes on the surface of the noble metals Au, Pd and Pt

A. Yakushev, W. Bröchle, E. Jäger, S. Reitmeier, E. Schimpf, M. Schädel, A. Shutov, S.N. Timokhin, A. Türler

Page 10

Development of an advanced version of the IVO-setup for future experiments with elements 112 and 114 *Page 12*

F.L. Haenssler, H.W. Gäggeler, S. Soverna, Z. Qin, R. Eichler, R. Dressler, D. Piquet

Volatilization behavior of transactinides from metal surfaces and melts *Page 13*

B. Eichler

The phenomenon of underpotential deposition - Comparison of radiochemical and electrochemical experiments in case of the deposition of Pb on Ag *Page 14*

H. Hummrich, J.V. Kratz

Influence of temperature and viscosity of the electrolyte on the kinetics of the electrodeposition of trace amounts of Pb on Pd electrodes *Page 15*

H. Hummrich, J.V. Kratz

Electrodeposition of ^{210}Po on Cu and Ag electrodes from various aqueous solutions and their mixtures with organic solvents *Page 16*

U. Rieth, J.V. Kratz

MICROSISAK-A New Device For Fast And Continuous Liquid-Liquid Extractions on a Microliter Scale

K. Eberhardt, S. Andersson, C. Ekberg, B. Horn, J.V. Kratz, A. Müller, M. Nilsson, G. Skarnemark, N. Trautmann

Page 17

Nuclear Structure

The search for ^{271}Mt via the reaction $^{238}\text{U} + ^{37}\text{Cl}$

Page 18

P.M. Zielinski, C.E. Düllmann, C.M. Folden III, P.K. Gupta, D.C. Hoffman, H. Mahmud, H. Nitsche, J.M. Schwantes, R. Sudowe, K.E. Gregorich, W.D. Loveland, D. Peterson, M. Schädel

^{20}Ne on ^{244}Pu – first preliminary results

Page 19

R. Dressler, B. Eichler, R. Eichler, A. Laube, J. Neuhausen, D. Piquet, H.W. Gäggeler, F.L. Haenssler, S. Soverna, Z. Qin, M. Schädel, E. Schimpf, K. Eberhardt, P. Thörle, N. Trautmann

Cross sections measurement in fusion reactions $^{36}\text{Ar}(^{148}\text{Sm};xn)$

Page 20

M. Schädel, W. Bröchle, E. Jäger, A.G. Popeko, S. Reitmeier, E. Schimpf, R. Sagaidak, A. Shutov, A. Türler, A. Yakushev, A.V. Yeremin

Atomic Physics with Heavy Ions

Towards the 1s Lamb Shift via Crystal Spectrometry

Page 22

H.F. Beyer, T. Stöhlker, D. Banas, D. Liesen, D. Protic, K. Beckert, P. Beller, J. Bojowald, F. Bosch, W. Bröchle, E. Förster, B. Franzke, A. Gumberidze, S. Hagmann, J. Hozzowska, P. Indelicato, O. Klepper, H.-J. Kluge, B. Kindler, S. König, C. Kozhuharov, B. Lommel, X. Ma, B. Manil, I. Mohos, A. Orsic Muthig, F. Nolden, U. Popp, A. Simionovici, D. Sierpowski, U. Spillmann, Z. Stachura, M. Steck, S. Tachenov, M. Trassinelli, N. Trautmann, A. Warczak, O. Wehrhan.

Indication for a gaseous element 112

S. Soverna for a Univ. Bern – PSI – GSI – Univ. Mainz – TUM – LBNL – UCB – IMP – collaboration

The expected relativistic stabilization of the closed-shell electronic ground state lead to the prediction of noble gas like properties for element 112 [1]. Other prediction methods yielded a volatile noble metallic character [2,3]. First chemical investigations yielded evidence that element 112 does not behave like Hg at room temperature. An upper limit of the adsorption enthalpy (ΔH_{ads}) of element 112 on gold was deduced as $-\Delta H_{\text{ads}}^{\text{Au}}(\text{E112}) < 60 \text{ kJ/mol}$. [4] Our experiment was designed to measure the adsorption enthalpy of element 112 on Au, which is decisive on whether it forms a metallic bond or a noble-gas like van der Waals interaction. So far, the only directly produced isotope of element 112 with a long enough half-life to be chemically characterised is $^{283}112$. Recent results [5] show that this isotope can be produced in the nuclear fusion reaction $^{238}\text{U}(^{48}\text{Ca},3n)$ with a cross-section of $\sim 2 \text{ pb}$. It decays via spontaneous fission with $t_{1/2} \sim 5 \text{ min}$. At the UNILAC accelerator at GSI Darmstadt a ^{238}U target was irradiated with about $2.8 \cdot 10^{18}$ particles of ^{48}Ca . Volatile products of the nuclear reaction were thermalized in pure He and swept through a PFA capillary to a getter oven containing Ta and Ti metal and operated at 1000°C in order to remove traces of water and oxygen from the carrier gas. Subsequently, the still volatile products were swept to the thermochromatographic device COLD. The adsorption behaviour of element 112 in the COLD detector was compared simultaneously with that of ^{185}Hg produced in the nuclear reactions of ^{nat}Nd (admixture to the target) with ^{48}Ca and of ^{220}Rn , a transfer-product of the reaction of ^{238}U and ^{48}Ca . A detailed description of the experimental set-up and the detection technique is given in [6]. The measured distribution of ^{185}Hg and ^{220}Rn is presented in Fig. 1. Applying a kinetic Monte-Carlo based model of gas adsorption chromatography, a quantification of the adsorption enthalpy of Hg and Rn is possible. The deposition pattern of Hg on Au allows the determination of a lower limit of $-\Delta H_{\text{ads}}^{\text{Au}}(\text{Hg}) < 80 \text{ kJ/mol}$, in good agreement with literature values [6]. The deposition pattern of ^{220}Rn is reproduced best assuming an adsorption enthalpy of $-\Delta H_{\text{ads}}(\text{Rn}) = 22 \pm 1 \text{ kJ/mol}$, indicating an ice coverage at the cold end of the detector array. Moreover, analysis of the time dependent change of the α -spectra resolution of the detector yielded evidence for an ice layer formation at temperatures below about -90°C (see Fig. 2). 11 high energy ($E > 35 \text{ MeV}$) events were measured during 16.8 days of experiment, at 3 expected background events. Their distribution along the detector array is presented in Fig. 2. A clear accumulation of 7 events was observed in the detectors #29-31. As no indications for actinide elements – possible transfer products of the ^{238}U with ^{48}Ca reaction – were found neither in the COLD nor in quartz wool filters situated just after the recoil chamber, most of the observed events have been tentatively assigned to the decay of $^{283}112$. Presumably caused by ice layer the measured energies of the 7 events were lower than expected. Therefore, we interpret our result only as an indication for the observation of SF $^{283}112$. A Monte-Carlo based statistical approach yielded the adsorp-

tion enthalpy of element 112 on ice surface $-\Delta H_{\text{ads}}^{\text{ice}}(\text{E112}) = 25 \pm 5 \text{ kJ/mol}$ (95% c.i.). Unfortunately, the adsorption of element 112 on ice does not allow conclusions about a chemical similarity either to Rn or to Hg. From the observed non adsorption of element 112 on gold down to temperatures of -90°C , an upper limit adsorption enthalpy of element 112 on Au $-\Delta H_{\text{ads}}^{\text{Au}}(\text{E112}) < 48 \text{ kJ/mol}$ was determined. This result reveals again a significantly weaker interaction of element 112 with Au compared to Hg.

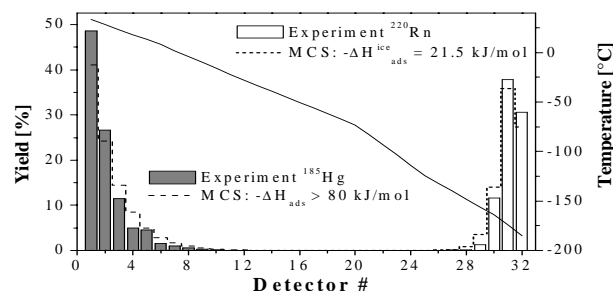


Fig. 1: Thermochromatogram of ^{185}Hg and ^{220}Rn (bars) measured along the detector array. Monte-Carlo simulations (dashed lines) are in good agreement with the experimental results. The temperature gradient is indicated (solid line).

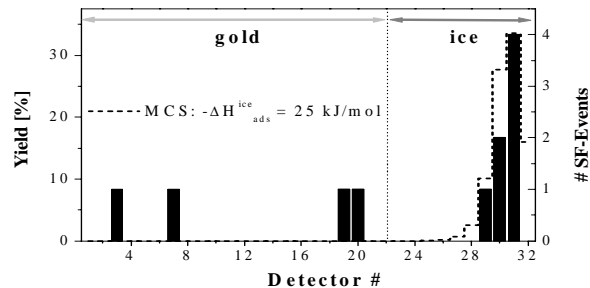


Fig. 2: Distribution of SF-fragments (black bars, right-hand scale) measured along the COLD. Monte-Carlo simulation is shown (dashed line, left-hand scale).

The upper limit of the adsorption enthalpy allows the estimation of an upper limit of the standard sublimation enthalpy of element 112 $\Delta H_{\text{(g)}}^0(\text{E112}) < 33 \text{ kJ/mol}$ [7], which is considered as a measure of its volatility. This result reveals element 112 to be more volatile compared to its homologue Hg and gaseous at standard conditions.

References

- [1] K.S. Pitzer, J. Chem. Phys. **63**, 1032 (1975).
- [2] B. Eichler, Kernenergie **19**, 307 (1976).
- [3] V. Pershina et al., Chem. Phys. Lett. **365**, 176 (2002).
- [4] A.B. Yakushev et al., Radiochim. Act. **91**, 433 (2003).
- [5] Yu.Ts. Oganessian et al., Eur. Phys. J. **A19**, 1 (2004).
- [6] S. Soverna et al., PSI Sci. Rep. *TEM* 2002, 65 (2003).
- [7] R. Eichler, PSI Sci. Rep. *TEM* 2003 (2004).

Theoretical predictions of the adsorption energy of element 112 on a gold surface

C. Sarpe-Tudoran^{*}, V. Pershina^{**}, B. Fricke^{*}, J. Anton^{*}, and W.-D. Sepp^{*}

^{*} Universität Kassel, D-34109 Kassel; ^{**} Gesellschaft für Schwerionenforschung, D-64291 Darmstadt

Recent discoveries of elements 112 through 116 have renewed the interest in the field of the superheavy elements (SHE). Element 112, first produced at the GSI, is of particular interest for chemical experiments: because of its closed electron shell and strongest relativistic effects it should exhibit properties similar to those of the noble gases. Thus, it was planned to study its volatility as adsorption on the gold surface of a chromatography column and compare it with the behaviour of the next nearest homologue Hg. To assist experimental investigations, adsorption of element 112 and Hg on gold is studied in the present work on the basis of fully relativistic density functional theory (DFT) electronic structure calculations.

From a theoretical point of view any surface can be considered as a huge molecule and the adsorption phenomenon as essentially local. We, therefore, approximate the surface by a gold cluster of moderate size. Taking into account the rest of the surface, this cluster is embedded in the potential produced by the atoms from the surrounding region.

In our DFT code [1], Vosko, Wilk and Nusair parameterization [2] is used for the exchange and correlation potentials. Nonlocal corrections are used perturbatively for exchange (with the relativistic form of RGGA of Becke's [3] approximation) and correlation (Perdew functional) [4] (B88/P86 in the tables), as well as the Perdew-Wang [5] for both exchange and correlation functionals (PW91/PW91 in the tables).

Calculations were performed for minimal and optimized atomic basis sets used previously in our calculations for the HgAu and 112Au dimers. The optimized basis includes additional functions $6p$ and $5f$ for Au and Hg, and $7p$ and $6f$ for element 112 on top of the minimal basis.

System	Binding energy E_b [eV]		
	RLDA	B88/P86	PW91/PW91
$HgAu_{14}$	-1.05	-0.45	-0.55
$112Au_{14}$	-0.58	0.03	-0.07
$HgAu_{34}$	-0.78	-0.18	-0.27
$112Au_{34}$	-0.37	0.23	0.13

Table 1: Binding energy of Hg and element 112 on the embedded Au clusters in the top position, when minimal neutral atomic basis sets are utilized.

First we performed computations for the top position, with the inner cluster simulated by 14 and 34 atoms using minimal basis sets. To estimate occupation number of the atoms of the surrounding cluster, we used the copy method described in [1]. An analysis of the results presented in Table 1 shows that the binding energy (E_b) decreases with increasing cluster size from 14 to 34 atoms (for the top position of the ad-atom relative to the surface). The difference in the binding energies ($\Delta E_b = E_b^{Hg} - E_b^{112}$) decreases from 0.47 eV to 0.41 eV, respectively. Results show

that Hg is weakly bound and element 112 is even unbound for the GGA values for $112Au_{34}$.

System	Binding energy E_b [eV]		
	RLDA	B88/P86	PW91/PW91
$HgAu_{14}$ (top)	-1.79	-1.14	-1.24
$112Au_{14}$ (top)	-1.23	-0.58	-0.68
$HgAu_{22}$ (hollow)	-2.57	-1.26	-1.44
$112Au_{22}$ (hollow)	-1.89	-0.67	-0.83

Table 2: Binding energy of Hg and element 112 on the embedded Au clusters, when optimized atomic basis sets are utilized.

For the optimized bases sets, the results in Table 2 show a significant increase of 0.69 eV and 0.61 eV in the binding energies of Hg and element 112 on the Au_{14} cluster, respectively. E_b^{Hg} is now much closer to the experimental value of 1.05 eV (101 kJ/mol [6]). This leads to an increase in ΔE_b from 0.47 eV to 0.56 eV. In the case of the hollow position of the ad-atom, this difference is about 0.6 eV. Thus, the influence of the potential created by the surrounding can be seen in the increased binding energies and in their enlarged difference between Hg and element 112. It may, however, happen that with the further increase of the Au-cluster size ΔE_b will be smaller, as is the case of MAu_{34} with respect to MAu_{14} for the neutral basis sets.

Comparison of the present data with our previous results [7] shows that obviously not a full convergence for the binding energies has previously been obtained due to the missing effects of the cluster surrounding.

On the basis of the present calculations, we can predict ΔH_{ads}^{112} on gold as ~ 0.5 eV with respect to the measured ΔH_{ads}^{Hg} of 1.05 eV [6].

References

- [1] T. Jacob, D. Geschke, S. Fritzsche, W.-D. Sepp, B. Fricke, J. Anton, S. Varga, *Surf. Sci.* **486**, (2001) 194.
- [2] S. H. Vosko, L. Wilk, M. Nusair, *Can. J. Phys.* **58**, (1980) 1200.
- [3] A. D. Becke, *Phys. Rev. A* **38**, (1988) 3098.
- [4] J. D. Perdew, *Phys. Rev. B* **22**, (1986) 8822.
- [5] J. P. Perdew, *Electronic Structure of Solids*, ed. by P. Ziesche and H. Eschrig, p. 11, Akademie Verlag, Berlin 1991.
- [6] J.-P. Niklaus, R. Eichler, S. Soverna, H. W. Gäggeler, *PSI Annual Report*, (2000) 8.
- [7] Cristina Sarpe-Tudoran, V. Pershina, B. Fricke, J. Anton, W.-D. Sepp and T. Jacob, *Eur. Phys. J. D*, **24**, 65-67 (2003).

Empirical Relation between the Adsorption Properties on Gold Surfaces and Volatility of the Elements 112 and 114

R. Eichler^{1,2}

¹PSI, Switzerland; ²University Bern, Switzerland

The typical result of gas phase chemical investigations on a one-atom-at-a-time level are standard adsorption enthalpies (ΔH_{ads}) of chemical species on stationary chromatographic surfaces. The standard adsorption enthalpies are deduced from experimental results using either the model of linear gas chromatography assuming mobile adsorption [1] or Monte-Carlo based models [2]. The obtained enthalpy values are independent on experimental conditions. The absolute amounts of these enthalpies represent the strength of interaction of the species with the surface. For example the deposition temperatures represent a comparable measure for this interaction strength only in the case of comparable experimental conditions. Thermochemical data describe collective properties of macroscopic amounts of the chemical species. Hence, links are needed for the derivation of thermochemical data from the experiments with single atoms. Nowadays, the only links are empirical correlations between ΔH_{ads} and collective data related to evaporation or sublimation as boiling points (b.p.) or standard sublimation enthalpies (ΔH_{subl}) of the type (eqn. 1):

$$-\Delta H_{\text{ads}} = A \cdot \Delta H_{\text{subl}} + B \quad (1)$$

The other way around, these correlations are used to predict the behavior of new chemical species in gas phase chemical adsorption studies using predicted thermochemical properties of these elements or compounds (see [3] for review). Empirical correlations as (eqn. 1) are established for chlorides and oxychlorides, oxides, and hydroxides, and for elements on quartz surfaces [3]. These correlations presuppose small or comparable netto adsorption enthalpies for all species on the respective stationary phase. Recently, the gas phase chemical investigation of the new transactinide p-elements are focused on the determination of the adsorption properties of their elemental state on noble metal surfaces. Especially, the elements 112 and 114 are expected to be very inert. Their metallic character is assessable only in the interaction with strongly oxidizing agents or in contact with noble metal surfaces. Hence, for the design of gas phase chemical experiments with these elements and for the data analysis of experimental results empirical correlations similar to that described above are indispensable. Here we present a correlation between the standard adsorption enthalpy of various elements on gold surfaces ($-\Delta H_{\text{ads}}(\text{Au})$) and their standard sublimation enthalpy at 0 K ($\Delta H^0(\text{g})$) (see Fig. 1). Other models can be used to describe directly the adsorption interaction of these elements on metal surfaces or to predict standard sublimation enthalpies. We use this correlation in order to predict the adsorption properties of the elements 112 and 114 in the experiments and to derive thermochemical data from first experimental results for element 112 [3][4] (see Table 1). Either $-\Delta H_{\text{ads}}(\text{Au})$ is given for the element due to various predictions or $\Delta H^0(\text{g})$. The given correlation is used to derive the corresponding value.

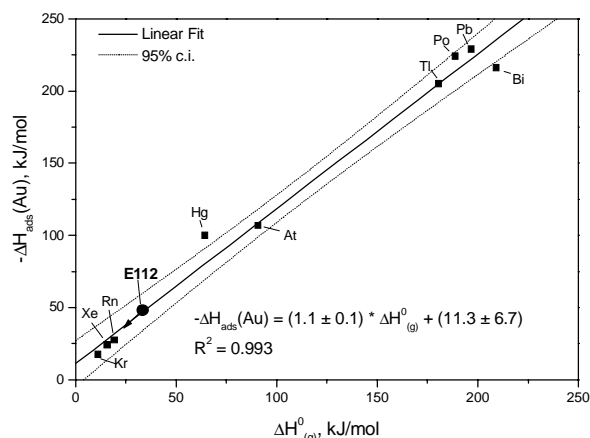


Fig. 1: Correlation between $-\Delta H_{\text{ads}}(\text{Au})$ and $\Delta H^0(\text{g})$ (black squares). The upper limit experimental result for element 112 [3] is shown (black dot).

Table 1: Summary of predicted data (bold) together with the corresponding calculated data (eqn. in Fig. 1).

Element	$-\Delta H_{\text{ads}}(\text{Au})$, kJ/mol	ΔH^0_{subl} , kJ/mol	Lit
112	35	22	[5]
112	38-60	25-44	[6]
112	53	38	[6]
112	80	63	[7]
112	-82	-85	[8]
112	30	17	[9]
112	34.4	21	[10]
112exp	≤60	≤44	[11]
112exp	<48	<33	[4]
114	90	71.5	[5]
114	143	120	[6]
114	220	190	[6]
114	60	44	[9]
114	35.5	22	[10]

References

- [1] B. Eichler et al., *Radiochim. Acta* **30**, 233(1982).
- [2] I. Zvara et al., *Radiochim. Acta* **38**, 95 (1985).
- [3] B. Eichler et al., In *Chemistry of Superheavy Elements*, Ch. 6, pp.205, Kluwer Academic Publishers, 2003.
- [4] S. Soverna et al., see this report.
- [5] B. Eichler, *Kernenergie*, **19**, 307 (1976).
- [6] B. Eichler, PSI Report 00-09/03-01; Villigen, 2000/2003.
- [7] V. Pershina, *J. Chem. Phys. Lett.*, **365**, 176 (2002).
- [8] G.V. Ionova et al. *Radiochemistry* **37(4)**, 282 (1995).
- [9] R. Eichler, et al., *J. Phys.Chem.* **B106**, 5413 (2002).
- [10] R. Eichler et al., PSI Annual Report 2003 8 (2004).
- [11] A.B. Yakushev et al., *Radiochim. Acta* **91**, 433 (2003).

Relativistic Effects on the Electronic Structure and Volatility of Group-8 Tetroxides MO_4 , where $\text{M} = \text{Ru}, \text{Os},$ and Element 108, Hs

V. Pershina¹, T. Bastug², B. Fricke³

¹GSI, Darmstadt; ²The Australian National University, Canberra

³Theoretische Physik, Universität Kassel, Kassel

Recently, first chemical experiments were conducted with the heaviest element Hs by studying volatility of its tetroxide, HsO_4 [1]. HsO_4 was shown to behave similarly to OsO_4 , though being adsorbed at somewhat larger temperatures. Earlier, fully relativistic DFT calculations [2] were performed indicating similarity of properties between OsO_4 and HsO_4 . To show the influence of relativistic effects on the electronic structures and volatility of the group-8 tetroxides, non-relativistic calculations for MO_4 ($\text{M} = \text{Ru}, \text{Os}, \text{Hs}$) were performed in addition to our previous relativistic ones [2]. Non-relativistic adsorption enthalpies of MO_4 on the quartz surface of the chromatography column have been predicted on their basis. Results are visualized in Figs. 1-3.

Relativistic effects on the d-orbitals only enhance orbital effects. As expected, relativistic effects increase the binding energy (D_e) in HsO_4 essentially, so that the trends in D_e for group-8 tetroxides become opposite for relativistic and non-relativistic values. Relativistic and non-relativistic polarizabilities show similar trends, since molecular bonding is determined by the d orbitals. Non-relativistically, polarizability of HsO_4 is the largest. Since $\alpha \sim 1/\text{IP}^2$, ionization potentials show trends opposite to those of α . The trends are similar for the relativistic and non-relativistic values, though relativistic effects dramatically increase IP of HsO_4 .

The energy of the dispersion interaction of MO_4 with the quartz surface is defined via the following equation

$$E(x) = -\frac{3}{16} \left(\frac{\epsilon - 1}{\epsilon + 2} \right) \frac{\alpha_{mol}}{\left(\frac{1}{\text{IP}_{slab}} + \frac{1}{\text{IP}_{mol}} \right) x^3} \quad (1)$$

Using the calculated relativistic and non-relativistic values, trends in relativistic and nonrelativistic $E(x)$ are defined as those shown in Fig. 3. They are similar for both relativistic and non-relativistic values.

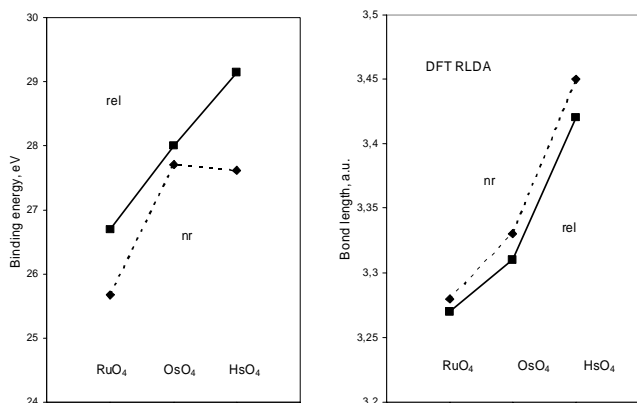


Fig. 1 Relativistic and non-relativistic binding energies (D_e) and bond lengths (R_c) in MO_4 ($\text{M} = \text{Ru}, \text{Os}$ and Hs).

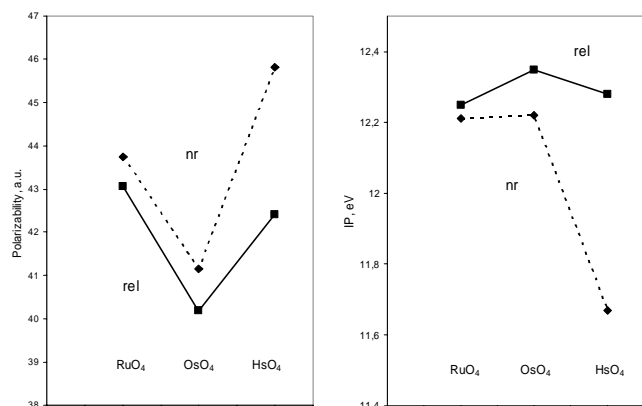


Fig. 2. Relativistic and non-relativistic polarizabilities (α) and ionization potentials (IP) in MO_4 ($\text{M} = \text{Ru}, \text{Os}$ and Hs).

Trends for both relativistic and non-relativistic bond lengths (R_c) were shown to be the same. This is due to the fact that trends in the spatial distribution of the relativistic and non-relativistic d orbitals are similar from Ru to Os and to Hs:

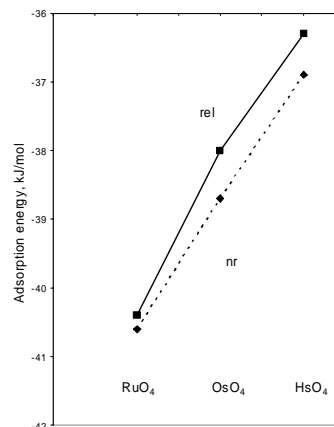


Fig. 3. Relativistic and non-relativistic adsorption energies of MO_4 ($\text{M} = \text{Ru}, \text{Os}$ and Hs) on quartz surface.

This is due to the fact that relativistic effects on α and IP cancel each other in eq. (1) and the trends are determined by x , the distance of MO_4 to the surface. It is taken proportional to the size of the molecules changing similarly for relativistic and non-relativistic values from Ru to Hs. Thus, relativistic effects increase volatility of each compound by about a couple of kJ/mol, but do not influence the trend for group-8 tetroxides.

References

- [1] C. Düllman *et al.* Nature (Letters), **418**, 859 (2002).
- [2] V. Pershina *et al.* J. Chem. Phys. **115**, 792 (2001).

Predictions of Adsorption Temperature for the Heaviest Elements and a Measure of Volatility

V. Pershina
GSI, Darmstadt

Our previous theoretical work to assist gas-phase chromatography experiments was limited to predictions of interaction energies of volatile species with the surface of a chromatography column [1]. This is, indeed the most important value. We, however, moved further and considered thermodynamics of adsorption in order to deduce equations to predict the adsorption temperature, T_{ads} , of a heaviest element/compound (B) with respect to T_{ads} of a lighter homolog (A). As a result, relevant equations are offered based on models of mobile and localized adsorption. As an example, adsorption of OsO_4 and HsO_4 on the quartz surface of a chromatography column is considered.

In the isothermal chromatography $T_{\text{ads}}(\text{B})$ of a heaviest element in relation to $T_{\text{ads}}(\text{A})$ at the established adsorption-desorption equilibrium (the peak of the temperature distribution curve) is usually measured. For a comparative study one can write a condition when their adsorption/desorption equilibrium constants are equal, i.e., $K_A(T_A) = K_B(T_B)$, or using statistical thermodynamics

$$e^{-\Delta E_A / RT_A} \frac{Q_A^s}{Q_A^g} = e^{-\Delta E_B / RT_B} \frac{Q_B^s}{Q_B^g}, \quad (1)$$

where $\Delta E_{A/B} = \Delta H_{\text{ads}}$ is the adsorption energy (enthalpy) of a species A or B, and $Q_{A/B}$ is their partition function for solid (s) and gas (g) phases. Taking into account that experiments for the heaviest elements and their homologs are conducted in the same set up under the same conditions and often simultaneously, final equations depend only on properties of the adsorbate and on its interaction with the adsorbent, i.e.

$$e^{-\Delta E_A / RT_A} \frac{1}{t_{1/2}^A r_A d_A^3 T_A m_A^{1/2}} = e^{-\Delta E_B / RT_B} \frac{1}{t_{1/2}^B r_B d_B^3 T_B m_B^{1/2}} \quad (2)$$

for the case when the molecule loses all the rotational degrees of freedom upon adsorption, or to

$$e^{-\Delta E_A / RT_A} \frac{1}{t_{1/2}^A r_A d_A T_A^{1/2} m_A^{1/2}} = e^{-\Delta E_B / RT_B} \frac{1}{t_{1/2}^B r_B d_B T_B^{1/2} m_B^{1/2}} \quad (3)$$

for the case when the molecule has one rotational degree of freedom in the adsorbed state. Here, r is the radius of a free molecule, d is the M-O distance, $t_{1/2}$ is half-life and m is mass.

As a proof of the validity of the model, ΔH_{ads} was calculated via eqs. (2,3) from the experimental $T_{\text{ads}}(\text{HsO}_4)$ of 229 K. Results of Table 1 show that predictions of $\Delta H_{\text{ads}}(\text{HsO}_4)$ via eq. (2,3) from experimental T_{ads} are in perfect agreement with those obtained via thermodynamical models and Monte-Carlo simulation [2]. Using the predicted by us $\Delta H_{\text{ads}}(\text{HsO}_4) = -36.3$ kJ/mol [1], $T_{\text{ads}}(\text{HsO}_4) = 183$ -184 K on the quartz surface has

been obtained, as is shown in Table 1. An analysis of the contribution of various properties of the adsorbate such as molecular weight and size shows that they should not be ignored in accurate determinations of ΔH_{ads} or T_{ads} .

Table 1. Adsorption enthalpies (ΔH_{ads}) and temperatures (T_{ads}) for OsO_4 and HsO_4 .*

MO ₄	T _{ads} , K	ΔH _{ads} , kJ/mol	T _{ads} , K	ΔH _{ads} , kJ/mol	ΔH _{ads} , kJ/mol
	predicted from calc. [1]		experiment [2]		from T _{ads} (exp.) via eqs. (2,3)
OsO ₄	191	-38.2	191	-38.2	-38.2
HsO ₄	184 ^a	-36.3	229	-44.9 ^c	-44.7 ^e
	183 ^b			-46 ^d	-45.6 ^f

^acalculated in this work via eq. (2) without rotational degrees of freedom for $\Delta H_{\text{ads}}(\text{HsO}_4) = -36.3$ kJ/mol and $t_{1/2} = 11$ s; ^bcalculated in this work via eq. (3) with rotational degrees for $\Delta H_{\text{ads}}(\text{HsO}_4) = -36.3$ kJ/mol and $t_{1/2} = 11$ s; ^cusing thermodynamics; ^dvia Monte Carlo simulation; ^ecalculated in this work via eq. (2) without rotational degrees of freedom for $T_{\text{ads}}(\text{HsO}_4) = 229$ K and $t_{1/2} = 11$ s; ^fcalculated in this work via eq. (3) with rotational degrees for $T_{\text{ads}}(\text{HsO}_4) = 229$ K and $t_{1/2} = 11$ s. * Experimental error bars are not shown in the table.

Finally, on the basis of eqs. (2,3) a more strict measure of volatility is suggested - a ratio of the desorption constants of homologous species at a given temperature

$$b' = \frac{K_{\text{desorp}}^B}{K_{\text{desorp}}^A} = \frac{m_B^{1/2} r_B d_B}{m_A^{1/2} r_A d_A} e^{\frac{(\Delta E_A - \Delta E_B)}{RT}}. \quad (4)$$

For OsO_4 and HsO_4

$$b' = 1.25 e^{\frac{\Delta E_{\text{Os}} - \Delta E_{\text{Hs}}}{RT}}. \quad (5)$$

Eq. (5) indicates that even at equal interaction energies of OsO_4 and HsO_4 with the surface, HsO_4 will have a higher vapour pressure over the surface than OsO_4 due to its larger weight and size and, hence, should be more volatile. Using "experimental" $\Delta H_{\text{ads}}(\text{OsO}_4) = -38.2$ kJ/mol and the theoretically predicted $\Delta H_{\text{ads}}(\text{HsO}_4) = -36.3$ kJ/mol,

$$b' = 1.25 \exp(1.9 \text{ kJ mol}^{-1} / RT).$$

This gives $K_p(\text{HsO}_4) = 2.85 K_p(\text{OsO}_4)$ at $T = 278$ K, which means that HsO_4 should have almost three times a higher P_{mm} , i.e., it should be more volatile, than OsO_4 .

References

- [1] V. Pershina *et al.* J. Chem. Phys. **115**, 792 (2001).
- [2] C. Düllman *et al.* Nature (Letters), **418**, 859 (2002).

Final result of the CALLISTO-experiment: Formation of sodium hassate(VIII)

A. von Zweidorf¹, R. Angert¹, W. Bröchle¹, S. Bürger², K. Eberhardt², R. Eichler^{1,3}, H. Hummrich², E. Jäger¹, R. Jera², H.-O. Kling², J. V. Kratz², U. Krille², B. Kuczewski², G. Langrock², G. Lehr², M. Mendel², A. Nähler², A. Peil², V. Pershina¹, U. Rieth², M. Schädel¹, B. Schausten¹, E. Schimpf¹, H.-J. Schött¹, E. Stiel¹, P. Thörle², N. Trautmann², K. Tsukada⁴, N. Wiehl², G. Wirth¹

¹Gesellschaft für Schwerionenforschung, Darmstadt, ²Institut für Kernchemie, Johannes Gutenberg-Universität Mainz, ³now at PSI, Villigen, ⁴JAERI, Tokai

In October/November 2002 the CALLISTO-project led to a hassium chemistry experiment at the UNILAC, for which preliminary results have been previously reported [1,2].

For the data evaluation, a time window of five times the literature half-lives and an energy window of ± 150 keV around

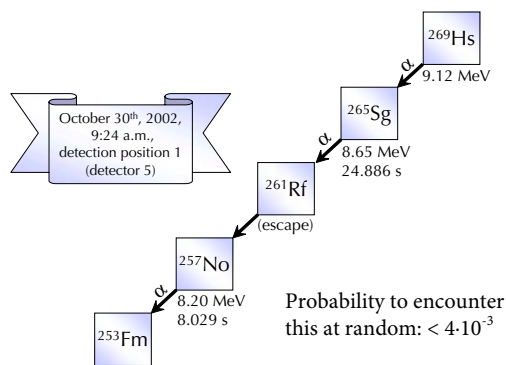


Fig. 1

the known α -decay energies were used. The recently published results, that ²⁶¹Rf decays with an α -decay energy of 8.52 MeV and a half-life of about 4.2 s, which is considered its ground state, were taken into account [3,4,5].

One correlated α - α - α decay chain and five α -SF decay chains were observed (Fig. 1 and 2).

Statistical considerations show, that these six events cannot be explained as background signals. The probability to encounter a random α - α - α -decay chain within the described time-energy-

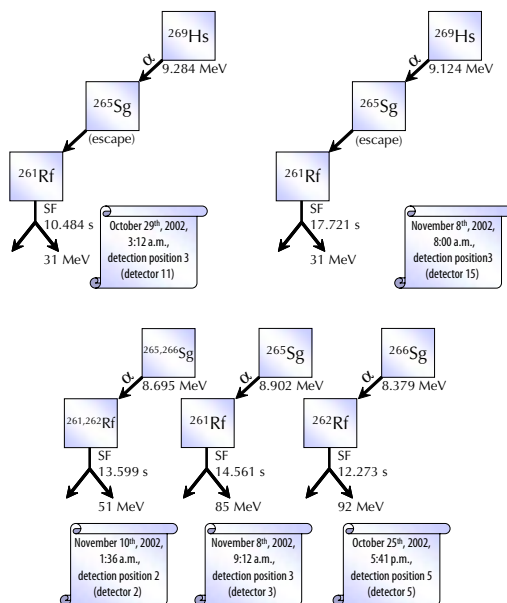


Fig. 2

window is below $4 \cdot 10^{-3}$. The probability to observe a SF-event after an α decay has occurred was calculated to one α -SF-correlation, based on the observed α -decay rate and the measured fission background.

The spatial distribution of Os and Hs in the described deposition and detection system [1,2] should depend on the interac-

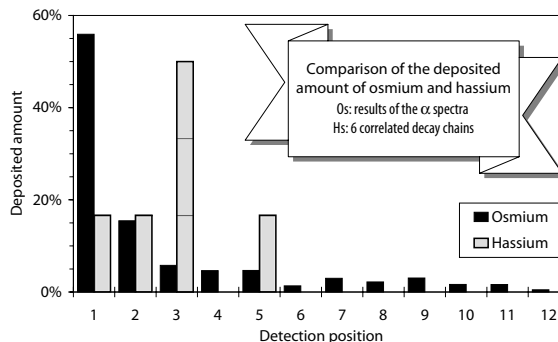


Fig. 3

tion of their tetroxides with the sodium hydroxide layer. In order to be able to investigate where the chemical reaction occurred, the data of all individual detectors had to be transformed. This is possible by defining a DETECTION POSITION, which is the position of detection relative to the gas inlet.

In this experiment, Os-isotopes and Hs-isotopes were produced simultaneously, the volatile OsO_4 as well as the volatile HsO_4 were synthesized in-situ and their deposition on NaOH in the presence of water was investigated. In the case of osmium, the formation of the osmate (VIII) is associated with a maximum at the first detection position (Fig. 3). The decay chains attributed to hassium decays were recorded in detection positions 1, 2, 3 and 5 (see Fig. 1 and 2 for the assignment of the individual decay chains). Since very similar properties of OsO_4 and HsO_4 can be expected, the deposition of hassium can be assumed to be the result of the formation of an analogous hassate (VIII) according to



The present experiment confirmed the formation and stability of the volatile HsO_4 [3]. In addition, from our results we conclude, that for the first time, an acid-base reaction was performed with the tetroxide of hassium leading to the formation of a hassate (VIII). Whether there is some evidence for a lower reactivity of hassium with respect to moisturized NaOH as compared to OsO_4 , remains an open question. Since only a few decay events were observed, further studies of the reactivity of HsO_4 would help to better characterize its chemical properties.

References

- [1] A. von Zweidorf *et al.*, GSI Scientific Report 2002, 175-177; pictures are available at <http://www.callisto.ws>
- [2] A. von Zweidorf, Gaschemische Untersuchungen in situ gebildeter flüchtiger Oxide des Rutheniums, Osmiums und Hassiums, Dissertation Johannes Gutenberg-University Mainz, Ibidem-Verlag Stuttgart, 2003 (ISBN 3-89821-315-3)
- [3] S. Hofmann *et al.*, Eur. Phys. J. A **14**, 147 (2002)
- [4] C. Düllmann *et al.*, Nature, **418**, 859 (2002)
- [5] A. Türler *et al.*, Eur. Phys. J. A **17**, 505 (2003)

Approaching first experiments with element 114

A.B. Yakushev¹, W. Bröchle², E. Jäger², E. Schimpf², M. Schädel², A. Türler¹, B. Wierczinski¹

¹ Institut für Radiochemie TUM, München, Germany

² Gesellschaft für Schwerionenforschung mbH, Darmstadt, Germany

Chemical studies of elements 112 and 114 will test "relativistic effects" in chemical properties and provide an independent determination of atomic number and decay properties of these elements. Element 114 was produced in $^{48}\text{Ca} + ^{242,244}\text{Pu}$ reactions and as daughter nuclides from element 116 isotopes synthesized with $^{245,248}\text{Cm}$ targets[1]. Of particular interest for us is the isotope $^{288}\text{114}$ ($T_{1/2} \approx 2$ s) obtained in the $^{244}\text{Pu}(^{48}\text{Ca}; 4n)$ reaction and as the daughter of $^{292}\text{116}$ produced in a $^{248}\text{Cm}(^{48}\text{Ca}; 4n)$ reaction.

From its ground state electronic structure, 114 belongs to group 14 of the Periodic Table. Its nearest homologue is Pb. Classical extrapolations predict 114 to behave as a metal with enhanced volatility compared to Pb. Relativistic quantum chemistry predicts stabilized spherical s and $p_{1/2}$ and destabilize $p_{3/2}$ - and d - orbitals. Consequently, the chemical behavior of 112 and 114 may approach the one of noble gases in volatility and chemical inertness[2]. The first experiments with 112 indicated qualitatively that 112 is chemically more inert than Hg[3]. However, for a first survey experiment on the chemistry of element 114, one needs to separate element 114 based on both predictions - classical extrapolations and relativistic calculations. Transporting 114 after its production in its elemental state directly to a detector setup, will be accompanied by large amounts of Rn (noble-gas-like behavior) and of Pb/Bi/Po activities (Pb-like behavior). On the other hand, 2-s $^{288}\text{114}$ is a little short-lived for its effective separation and detection. Therefore we are developing for the first experiment a combination of two processes: 1) synthesis and rapid chemical separation of 114 by adsorption on a noble metal surface, and 2) desorption, gas transportation and detection of 112 as a daughter nuclide after alpha-decay of element 114. This separates the volatile metals Pb, Bi and Po, as well as the noble gas Rn and allows a unique identification of 114 and 112.

The envisioned approach can be realized with two alternating steps using two columns one for adsorption and one for desorption (Fig. 1). In a first step, reaction products are transported by He or Ar gas from a recoil chamber to a column kept at "low" temperature. 114 should adsorb on a chemical active surface of the first column and gaseous Rn passes through the column with the flowing gas. Simultaneously, 112, as the 114 decay product, will be evaporated from the

second column kept at a high temperature and will be transported to a detection system by pure He gas flow. After a few seconds valves switch positions, the high-temperature column is cooled and the low-temperature column is heated fast. In a second step, 112 as the decay product of the adsorbed 114 is evaporated from the first column and adsorption of E114 takes place at the second column. This process is continuing as a two-step cycle.

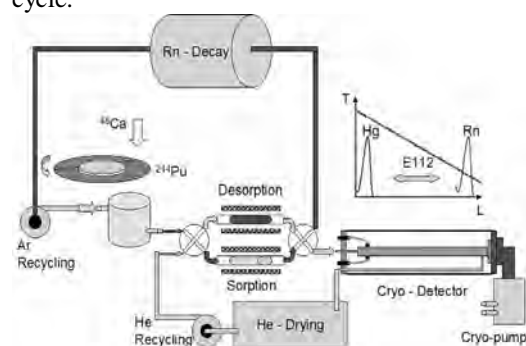


Figure 1. Schematic for a two-step chemical separation of E114 and E112.

To develop this approach we are performing test experiments on the gas chromatography of Pb, Hg and Rn to choose suitable materials for chemical filters and for the best temperature regime. Additionally, problems like a fast heating and cooling of the columns or drying of He gas have to be mastered. The water content in He should correspond to a dew point temperature of approximately -200°C . We propose to recycle the He and/or Ar flows in closed systems with purification stages. Additionally, a buffer volume will be installed in the Ar line to let the Rn decay. The detection system consists of a thermogradient channel formed from PIPS detectors kept at temperatures from 0 to -200°C . The detector assembly is placed in a vacuum enclosure. The high vacuum (10^{-6} - 10^{-7} mbar) is needed for a good vacuum thermoinsulation.

[1] Yu.Ts. Oganessian et al., Contribution to the 2nd Int. Conf. on the Chemistry and Physics of the Transactinide Elements, November 16-20, 2003, Napa, USA.

[2] P. Schwerdtfeger et al., *J. Nucl. Radiochem Sci.* **3**, 133(2002).

[3] A.B. Yakushev et al., *Radiochim. Acta* **91**, 433(2003).

Gas chromatography of short-lived Hg isotopes on the surface of the noble metals Au, Pd and Pt

A. Yakushev¹, W. Bröchle², E. Jäger², S. Reitmeier¹, E. Schimpf²,
M. Schädel², A. Shutov³, S.N. Timokhin³, A. Türler¹

¹ Institut für Radiochemie TUM, München, Germany

² Gesellschaft für Schwerionenforschung mbH, Darmstadt, Germany

³ Flerov Laboratory of Nuclear Reactions JINR, Dubna, Russia

The discovery of relative long-lived isotopes of superheavy elements in ⁴⁸Ca-induced reactions opens an opportunity for chemical studies with elements 108 to 114. The most interesting objects in such studies are elements 112 (E112) and 114 (E114) because of a possible manifestation of very strong relativistic effects in its chemical behaviour. Due to a very significant contraction of the valence electron shell, it seems to be spherical and very stable. First experiments with E112 [1] are in agreement with theoretical predictions indicating that E112 is much more inert than its nearest homolog Hg. For experiments with E114 we develop an approach based on the chemical adsorption of E114 on a suitable metal surface followed by the desorption and detection of its α -decay daughter E112[2]. To perform such an experiment we need to know the temperature region and the material at which Pb (and E114) are strongly adsorbed while Hg (and E112) is not. Results from theoretical calculations for metal-metal interactions between transactinides and transition metals[3] indicate that a group of noble metals are a good choice for the separation of E114 from E112. While E114 should exhibit an enhanced volatility and inertness compared to its homolog Pb, its reactivity or interaction with other metals is expected to be much stronger as compared with Hg or E112. To pursue such a goal we began studying adsorption-desorption processes of short lived Pb and Hg isotopes on Au, Pd and Pt surfaces.

Short-lived Pb isotopes were produced in fusion reactions using ³⁶Ar beam (7.38 MeV/u) from the UNILAC (GSI) and rotating Gd targets. ¹⁵²Gd (30% enriched) and ^{nat}Gd targets (1 mg/cm² on 10 μ m Be foils), respectively, were mounted on a the rotating target wheel ARTESIA. Reaction products were flashed out from a recoil chamber by He at a gas flow of 1 l/min direct into a quartz column, which was kept at different temperatures from room temperature up to 1000°C. As a chromatographic column we used (i) an open quartz column and (ii) quartz columns

with inserts: quartz wool plug or metal foils. The quartz wool plug was inserted at the high temperature position, 20 cm apart from the column inlet. The Au, Pd and Pt foils were rolled as tubes of 20 cm in length and inserted into the columns. Volatile products were transported from the chromatographic column to a detector through a Teflon capillary of 2 mm i.d. The transportation time was 3 s. The detector consisted of 4 pairs of PIPS detectors with an area 18x18 mm² each, covered with thin gold layers. The gap between the top and bottom detectors was about 1 mm (Fig.1).



Fig.1. View of the opened detector.

Our goal was optimising the yield of short-lived Hg isotopes after alpha decay of Pb isotopes produced in fusion reactions. Unfortunately we couldn't maximise the Pb yield because our recoil chamber was not heated. For experiments with the open quartz column or the quartz column with a quartz wool plug, the yield of Hg isotopes was constant over the whole temperature range and was equal to the maximal yield obtained in tests with metal columns.

Gas chromatography yields of ^{182,185}Hg on noble metal columns and results from Monte Carlo simulations are shown in Figures 2-4. The chromatograms on Au, Pd and Pt foils look different. However, we couldn't describe the experimental data obtained in the tests using Au

and Pd columns with a mobile adsorption mechanism only. We calculated two limits (left and right curves) well describing our experimental data.

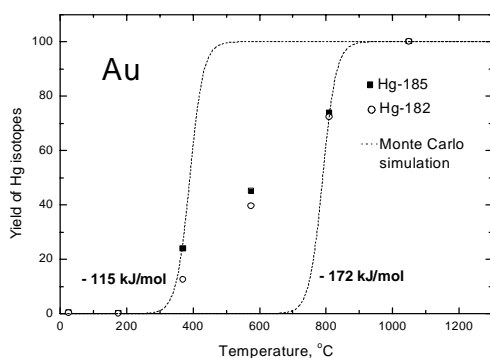


Fig.2. Adsorption of $^{182,185}\text{Hg}$ on the Au surface.

One possible explanation for this non model-like behavior may be diffusion of Hg atoms into the metal matrix at higher temperatures. Thus, longer times (reflected in higher temperatures) are needed to bring atoms to the surface again before they desorb. Therefore, the left calculated curves in the Fig. 2 and 3 characterize a pure adsorption-desorption process only.

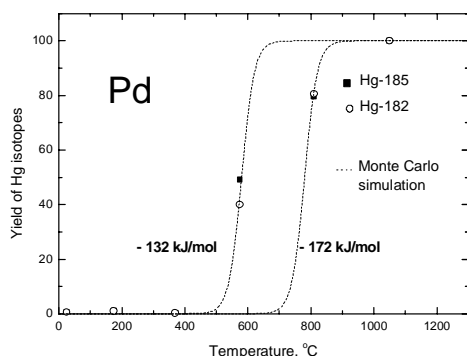


Fig.3. Adsorption of $^{182,185}\text{Hg}$ on the Pd surface.

Desorption of Hg atoms from a Pt surface occurs at much lower temperature, and, obviously, no diffusion into the material takes place. Based on our experimental data, the adsorption strength of Hg on noble metal surfaces increases from Pt to Pd: $\text{Pt} < \text{Au} < \text{Pd}$.

As the Au surface had no oxide layer, Hg was adsorbed quantitatively at room temperature without any surface pretreatment. To remove oxide layers from the Pd and Pt surfaces, we needed to heat these metal foils up to 1000°C before the experiment. After such a pretreatment a quantitative adsorption of Hg on Pd and Pt was measured at room temperature, too.

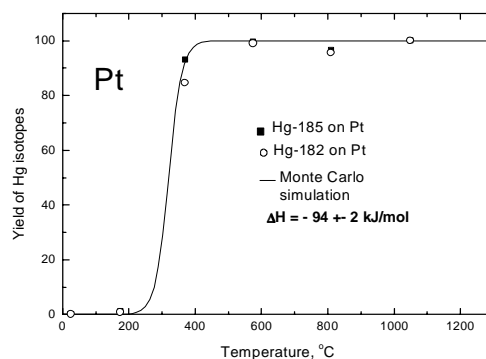


Fig.4. Adsorption of $^{182,185}\text{Hg}$ on the Pt surface.

Thermochromatographic experiments with Pb performed at FLNR[4] and PSI[5] confirmed a very strong metal-metal interaction between Pb and noble metals. The adsorption temperature of Pb on the quartz surface was about 600°C , whereas Pb was adsorbed on the Pt surface at temperatures $\geq 1050^\circ\text{C}$. It is well known, that adsorption of Pb on quartz is accompanied by the oxidation of Pb from oxygen atoms of quartz. However, the interaction between Pb and Pt or other transition metals is much stronger. This first comparative study of Pb and Hg adsorption on noble metals indicates to select Pt as a column material for Pb-Hg separation. On the other hand, one needs to heat the recoil chamber to relatively high temperatures of about 800°C to prevent losses of Pb-like products in the recoil chamber due to adsorption on the walls. The temperature regime has to be optimized in upcoming experiments.

The authors thank Prof. B. Eichler for helpful discussions.

[1] A.B. Yakushev et al., *Radiochim. Acta* **91**, 433(2003).

[2] A. Yakushev et al., this Annual Report.

[3] B. Eichler, PSI Bericht 00-09 (2000), PSI Bericht 03-01 (2001), PSI Villigen, Switzerland.

[4] S.N. Timokhin, private communications.

[5] Z. Qin et al., Contribution to the 2nd International Conference on the Chemistry and Physics of the Transactinide Elements (TAN03), November 16-20, 2003, Napa, USA.

Development of an advanced version of the IVO-setup for future experiments with elements 112 and 114

F.L. Haenssler¹, H.W. Gäggeler^{1,2}, S. Soverna¹, Z. Qin¹, R. Eichler^{1,2}, R. Dressler², D. Piguet²

¹PSI, Switzerland; ²University Bern, Switzerland

Relativistic effects are believed to be very strong in the region of the super heavy elements, thus, strongly affecting their chemical properties. According to their position in the periodic table, elements 112 and 114 should behave like noble metals but a noble gas character induced by the relativistic effects can not be excluded. Relatively stable isotopes of elements 112 and 114 were produced in Dubna with ^{48}Ca induced fusion reactions using ^{238}U and $^{242,244}\text{Pu}$, respectively, as targets [1]. A first experiment to investigate the chemical properties of element 112 was performed in February and March 2003 [2] using $^{283}112$ ($T_{1/2} = 5$ min, SF [3]) produced in the nuclear fusion reaction of ^{48}Ca with ^{238}U . The produced isotopes were adsorbed and detected in the COLD thermochromatography device. The results indicated a very volatile element 112. A drawback of the experiment was the ice layer, formed in the cold part of the set-up, on which element 112 was absorbed. The adsorption enthalpies of Hg, Rn, and element 112 are too close to each other in order to make statements about similarity of element 112 either to Rn or to Hg. Although, the non adsorption of element 112 on the free gold surface down to temperatures of about -90°C yield evidence for its very inert and volatile behavior. The ice layer interfered also an unambiguous determination of the energy of the spontaneous fission fragments from the decay of $^{283}112$ [2]. Hence, the next steps towards a further experiment must be: 1. to improve the COLD device to a 4- π -detection system, 2. to tighten the device and 3. to decrease the water content in the carrier gas.

A 4- π -COLD system with gold covered PIN Diodes is under development at PSI. Hence, we used for the first test experiments the 2- π -COLD, as it was used during the experiments with element 112. A first approach to a carrier gas with lower water content is the use of a gas-loop (see Figure 1). In order to keep the amount of water as low as possible the whole set-up is evacuated before the experiment. Once the system is filled with Ar-gas, the pump, the pressure sensor, and the buffer provide a constant gas flow up to 1.5 l/min. Getter ovens (Ta, 1000°C) are used to keep the gas loop dry during the experiment. Additionally, the investigation of short lived nuclides of element 112, produced in the reaction of ^{48}Ca with ^{244}Pu via the decay of isotopes of element 114 require a very small recoil chamber of only about 9 ml volume. In order to stop the recoiling products of the nuclear reaction in such small volume, Ar is used because of its higher stopping power compared to pure He, which was used before. The buffer is used in order to reduce the pulsation in the carrier gas caused by the metal bellow pump. A trap filled with charcoal is used in the gas loop, in order to trap all Rn isotopes, which are able to pass the COLD detector.

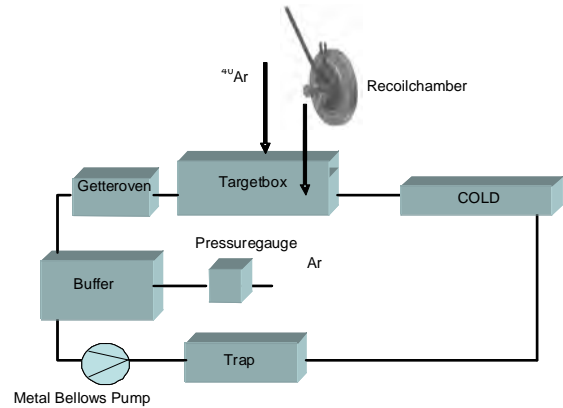


Fig. 1: Gas-loop set-up for future experiments with the elements 112 and 114

First experiments were done using ^{219}Rn ($T_{1/2} = 3.96$ s), which emanates from a ^{227}Ac -source. Rn was adsorbed at a temperature of about -180°C (see Figure 2). A Monte-Carlo simulation yielded an adsorption enthalpy of -20 kJ/mol, which is typical for the adsorption of Rn on ice.

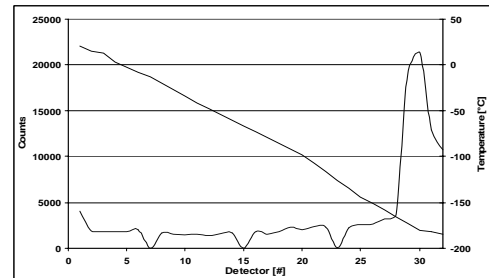


Fig. 2: Thermochromatogramm of ^{219}Rn on Gold/Ice

Notable is also the slight increase of in-flight decayed Rn at the beginning of the channel, which is probably induced by turbulences of the gas flow at the entrance of the COLD channel. The α -spectroscopic resolution in the last detectors remained in the order of 60 keV for more than 10 h experimental duration, indicating much less water content in the whole system compared to the experiments in [3]. Further experiments are envisaged at the PSI Philips cyclotron using model nuclides produced in the nuclear reaction $^{152}\text{Gd}(^{40}\text{Ar},6n)^{186}\text{Pb}(\alpha, 4.8\text{s}) \rightarrow ^{182}\text{Hg}(\alpha, 11\text{s})$.

References

- [1] Yu. Ts. Oganessian et al., Nucl. Pys., **A682**, 108 (2001).
- [2] S. Soverna et al., see this report.
- [3] Yu. Ts. Oganessian et al., Eur. Phys. J. A (2004).

Volatilization behavior of transactinides from metal surfaces and melts

B. Eichler¹

¹PSI, Switzerland

Volatilization properties of elements with the atomic numbers $Z=104$ to 116 are determined on the basis of empirical relations. These empirical correlations can be deduced from the analysis of thermochemical data of elements in the periodic table and their relations to the material constants. Structure specific connections are shown to exist between the electron densities at the “Wigner-Seitz” cell borders [1] of metals and the specific surface energies of solid metals with hexagonal, face-centred cubic, body-centred cubic and rhombohedral lattices. Analogously, structure specific relations can be found between the standard enthalpies of the gaseous monoatomic metals and their surface energies. Linear correlations with exceptionally high correlation coefficients are observed between the standard sublimation enthalpies of isotypic metals in the dimeric state and the surface energies [2]. Volatilization properties (see Fig. 1-5) have been deduced for the transactinoides on the basis of these established relations, applying predicted structures and electron densities of of transactinides.

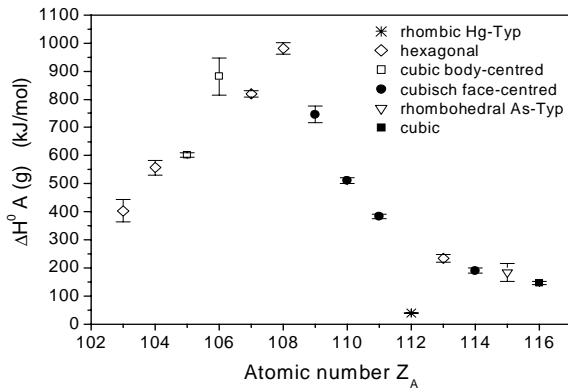


Fig. 1: Standard enthalpies of monoatomic elements

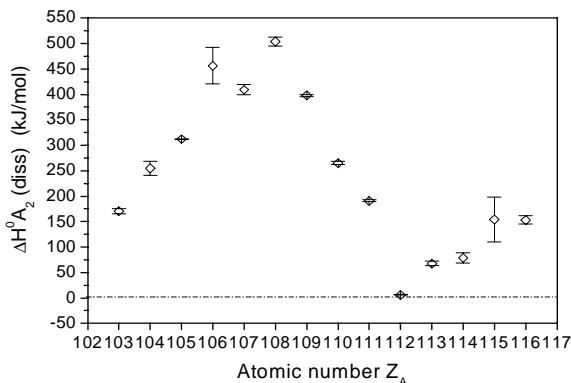


Fig. 2: Standard dissociation enthalpies of dimers

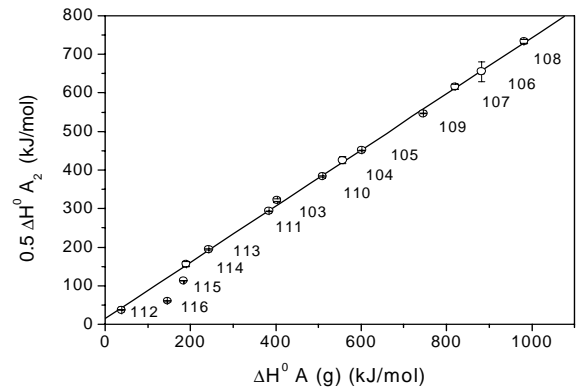


Fig.3: Comparison of sublimation enthalpies in the mono-atomic and the dimeric state

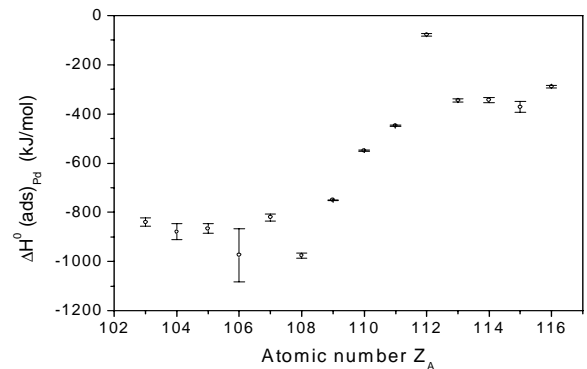


Fig.4: Adsorption enthalpies on Palladium

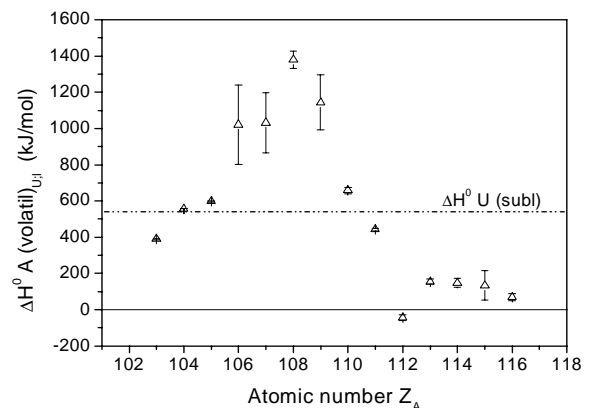


Fig.5: Enthalpies of volatilization from Uranium melt

References

- [1] B.Eichler, Metallchemie der Transaktinoide, PSI Bericht Nr. 00-09, Dezember 2000, ISSN 1019-0643.
- [2] B. Eichler, Verflüchtungsverhalten der Transaktinoide von Metalloberflächen und aus Schmelzen PSI Bericht Nr. 03-01 Januar 2003, ISSN 1019-0643.

The phenomenon of underpotential deposition - Comparison of radiochemical and electrochemical experiments in case of the deposition of Pb on Ag

H. Hummrich, J.V. Kratz

Institut für Kernchemie, Johannes Gutenberg-Universität Mainz

The electrochemical deposition of a metal A on an electrode B in the sub-monolayer regime occurs at more positive potentials as compared to the Nernst potential if the interaction of A with B is thermodynamically more advantageous than that of A with A.

In cyclic voltammetry, underpotential deposition (upd) becomes visible by a current peak occurring upon the deposition of the first monolayer on the electrode which is shifted positively relative to the peak associated with the deposition of the bulk. Hereby, the metal-ion concentration is in the mmol regime. By the use of radiotracers, on the other hand, one can carry out experiments in extremely diluted solutions. Even in case of a complete deposition of the tracer, one obtains electrode coverages that are much smaller than a monolayer. The detection of the deposited metal occurs via its radiation.

In order to compare electrochemically and radiochemically determined underpotentials, the deposition of Pb on Ag was investigated.

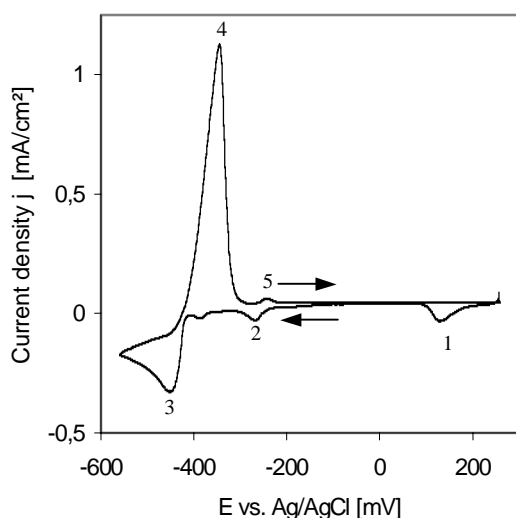


Fig. 1: Cyclic voltammogram of the Pb deposition on Ag. 10^{-4} mol/l Pb^{2+} in 0.1 M $HClO_4$. Scan: 10 mV/s, (1) deposition of dissolved Ag^+ , (2): deposition of the Pb monolayer, (3) deposition of the bulk (4) dissolution of the bulk (5) dissolution of the Pb-monolayer

For the cyclic voltammetry, a BANK M-Lab-100 potentiostat was used. The area of the Ag electrode was 2 cm². The Pt counter electrode was shielded by a glass frit in order to avoid a reaction of the Pb^{2+} with the counter electrode. The electrolyte (volume = 25ml). was made free of oxygen by purging with nitrogen. In Fig. 1, one observes the deposition and re-dissolution of the bulk and the monolayer.

For the radiochemical experiments, ^{212}Pb was used. The area of the Ag electrode was 1 cm²; a Pt counter electrode

and a Ag/AgCl reference electrode were used. The electrolyte (volume = 1ml) was stirred during electrolysis. Under these conditions, for the given potential, the maximum possible deposition was achieved in 5-10 min. Starting at positive potentials, electrolysis was continued for 10 min, the working electrode was removed and the deposited activity was determined by γ -spectrometry. Thereafter, the electrolysis was continued at a lower potential etc.

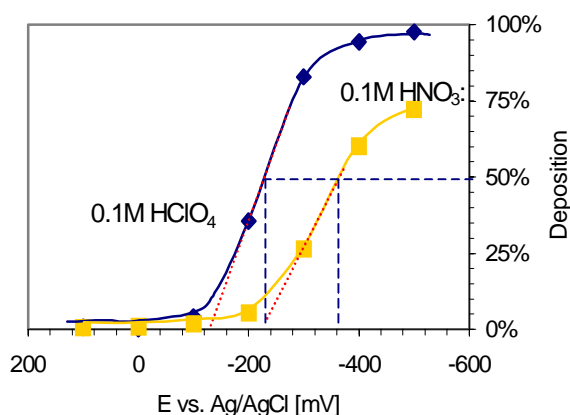


Fig.2: Deposition of ^{212}Pb on Ag from 0.1 M $HClO_4$ and 0.1 M HNO_3 . The crossings of the tangents with the x-axis give the critical potentials, the dashed lines indicate the potentials at 50% deposition.

Starting at a critical potential (E_{crit}), the deposition sets in and approaches eventually 100% (Fig. 2). Apart from E_{crit} , from the potential curve, the potential for 50% deposition ($E_{50\%}$) can be deduced.

Table 1: Comparison of upd potentials for the deposition of Pb on Ag from 0.1 M $HClO_4$

	E vs. Ag/AgCl [mV]
<i>Cyclic voltammetry</i>	
Deposition of Pb monolayer	-280
Dissolution of Pb monolayer	-254
<i>Radiotracer method</i>	
$E_{50\%}$ (Pb/Ag)	- 230
E_{crit} (Pb/Ag)	- 130

The potential for the dissolution of the Pb monolayer (-254 mV) agrees with that measured by Kolb in 1 M $NaClO_4$ (pH3) which is -255 mV [1]. Table 1 shows that the $E_{50\%}$ -value is not too far from the upd potential determined by cyclic voltammetry.

References

- [1] D.M. Kolb, M. Przasnyski, H. Gerischer, J. Electroanal. Chem. **54**, 25 (1974)

Influence of temperature and viscosity of the electrolyte on the kinetics of the electrodeposition of trace amounts of Pb on Pd electrodes

H. Hummrich · J.V. Kratz

Institut für Kernchemie, Johannes Gutenberg-Universität Mainz, Germany

In order to use electrodeposition as a separation method for short lived radioisotopes, the electrochemical deposition must occur rapidly. Therefore, it is necessary to investigate the relevant parameters determining the deposition kinetics.

According to Joliot [1], the electrochemical deposition of radiotracers is determined by

$$\frac{dN_{\text{dep}}}{dt} = \frac{DF}{\delta V} (KN_{\text{tot}} - N_{\text{dep}}) \quad (1)$$

Here, dN_{dep}/dt is the number of deposited atoms per time unit, N_{tot} is the total number of atoms in solution, D is the diffusion coefficient, δ the thickness of the Nernst diffusion layer, F the area of the electrode, and V the volume of the electrolyte. K stands for the maximum fraction of atoms that can be deposited at a given potential. A fast deposition can apparently be achieved by a large ratio of the area of the electrode to the volume of the electrolyte, a small Nernst diffusion layer (achievable by intensive convection) and by a large diffusion coefficient..

For $K = 1$, i.e. for sufficiently negative potential, one obtains after integration:

$$\ln\left(1 - \frac{N_{\text{dep}}}{N_{\text{tot}}}\right) = -\frac{DF}{\delta V} t \quad (2)$$

If the hydrated ion that is to be deposited is assumed to be spherical, the Stokes-Einstein equation applies:

$$D = \frac{kT}{6\pi\eta a} \quad (3)$$

where a is the hydrodynamical radius of the ion, η the dynamic viscosity of the solution, k the Boltzmann constant, and T the absolute temperature.

According to Fahland [2], one can define the time after which 50 % of the atoms in solution are deposited as $t_{50\%}$. If one replaces in eq. (2) the diffusion coefficient according to eq. (3), one obtains:

$$t_{50\%} = \frac{\ln 2 \cdot 6 \cdot \pi \cdot V \cdot a \cdot \delta \cdot \eta}{F \cdot k \cdot T} \quad (4)$$

High temperatures and low viscosities should lead to short values of $t_{50\%}$.

^{212}Pb was used as tracer in the deposition experiments. As working electrodes, Pd electrodes with an area of 1 cm^2 were used. The counter electrode was made of Pt. Electrolytes were 1 ml solutions of 0.1M HClO_4 , HCl , and HNO_3 . The solutions were agitated by a magnetic stirrer at 600 rpm. The potential was fixed by a potentiostat at -500 mV vs. the potential of a Ag/AgCl -electrode which allows for a maximum deposition with $K = 1$. The change of the potential of the reference electrode by an increase of the temperature amounts to $< 30 \text{ mV}$ which is too small to

influence the deposition significantly. The working electrode was removed under voltage from the solution at given time intervals and was measured by γ -spectrometry. The electrolysis was repeated at different temperatures

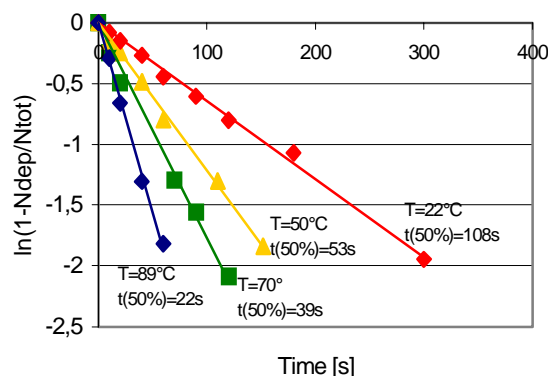


Fig. 1: Deposition of ^{212}Pb on Pd electrodes from 0.1 M HClO_4 as a function of the duration of the electrolysis and the temperature of the electrolyte.

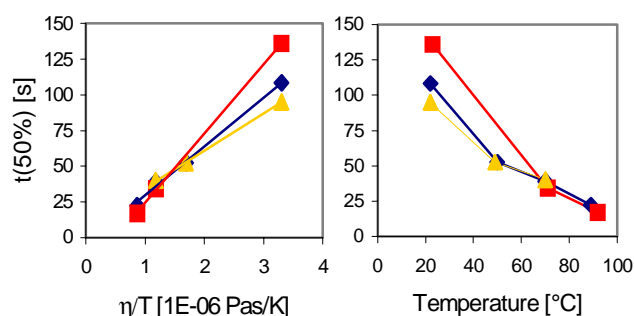


Fig. 2: $t_{50\%}$ as a function of the ratio of viscosity to temperature, or as a function of temperature (red: 0.1 M HCl , blue: 0.1 M HClO_4 , yellow: 0.1 M HNO_3)

The dependence of $t_{50\%}$ on the ratio of viscosity to temperature is linear as expected. A rise of the temperature is accompanied by a decrease of the viscosity of the solution. As in eq. (4), it is the influence of the viscosity that dominates: a rise of the temperature from $20 \text{ }^\circ\text{C}$ to $90 \text{ }^\circ\text{C}$ corresponds to an increase in the absolute temperature by a factor 1,2 ($293 \text{ K} \rightarrow 363 \text{ K}$), but leads to a decrease of the viscosity by a factor of 3,2 ($1 \text{ mPas} \rightarrow 0,315 \text{ mPas}$).

In future experiments, the usefulness of non-aqueous low-viscosity electrolytes (e.g. methanol, acetone) for the electrochemical deposition of radiotracers is to be investigated.

References

- [1] F. Joliot, J. Chim. Phys. **27**, 119 (1930)
- [2] J. Fahland, Doctoral Dissertation, Johannes Gutenberg-Universität Mainz (1960)

Electrodeposition of ^{210}Po on Cu and Ag electrodes from various aqueous solutions and their mixtures with organic solvents

U. Rieth, J.V. Kratz

Institut für Kernchemie, Johannes Gutenberg-Universität Mainz, D-55099 Mainz

In two series of experiments, yields of the spontaneous electrodeposition of polonium were measured. The carrier-free solutions of ^{210}Po in 0.1M HCl and in 0.1M HNO₃ were prepared as described in [1]. Those solutions were used either in their pure form or in a 1:1 mixture with organic solvents. Due to the addition of these solvents, one can influence the viscosity of the solution. By doing so, a direct effect on the deposition velocity can be achieved.

The experiments performed with the pure solution showed a clear advantage of the HCl solution in comparison with the nitric acid solution. As shown in fig. 1, the achieved yields with the 0.1M HCl after 5min of reaction time are already close to 100%. In contrast to this, only about 50% of the polonium was deposited from 0.1M HNO₃ under otherwise identical conditions (fig. 2).

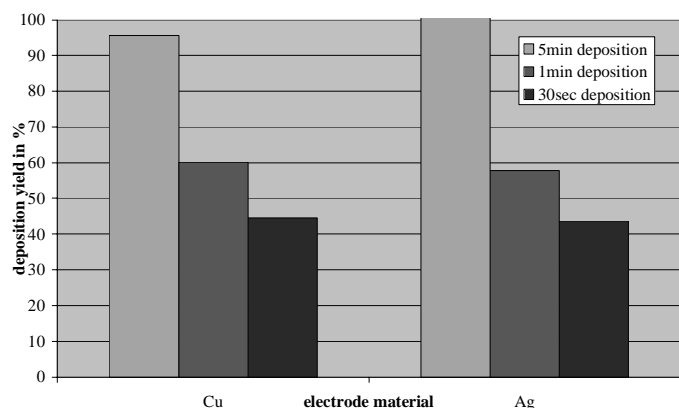


Figure 1: Deposition of ^{210}Po on Ag and Cu from 0.1M HCl.

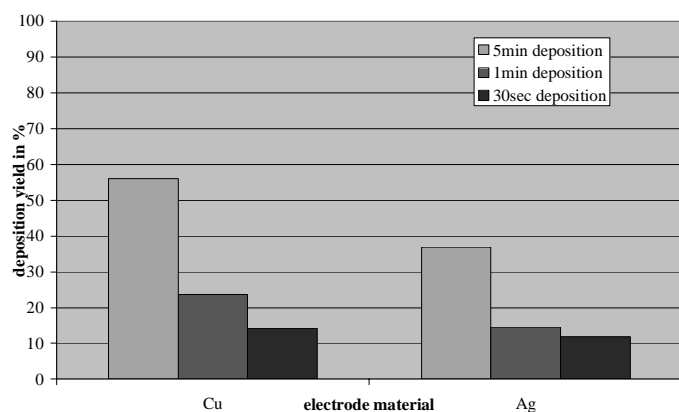


Figure 2: Deposition of ^{210}Po on Ag and Cu from 0.1M HNO₃.

As qualitative interpretation of this observation, the oxidizing properties of the nitric acid could be taken into account. This might prevent the necessary reduction step of the deposition of polonium ions from taking place. As a consequence the whole electrodeposition process is slowed down in nitric acid solution as compared to the HCl solution.

In the second series of experiments, the polonium solutions were mixed with 50-vol% of various organic solvents. These mixtures were contacted with the electrodes for 1min. From figure 3, one can see that these solvent additions have a strong effect on the deposition yields. While dioxane additions reduce the deposition yields due to an increase of viscosity, the addition of acetonitrile significantly increases the yields by reducing the viscosity of the solution.

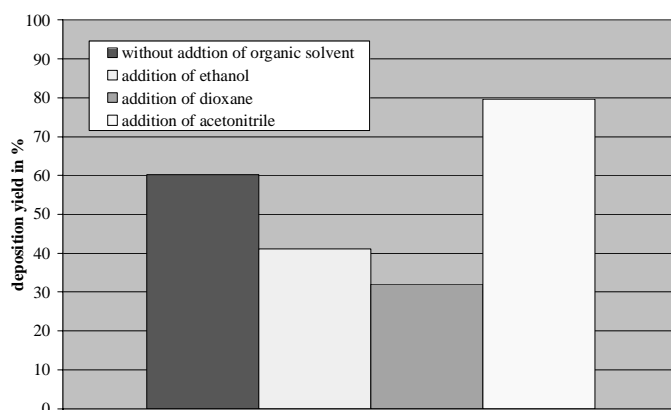


Figure 3: Deposition of ^{210}Po on Cu from 0.1M HCl with various organic solvents added.

These observations are in very good agreement with a theoretical consideration of Hummrich et al. [2] which shows that the time until a 50% deposition yield is reached is directly proportional to the viscosity of the solution.

References

- [1] U. Rieth et al., GSI, *Scientific Report 2002*, p.183.
- [2] H. Hummrich et al., GSI, *this report*.

MICROSISAK – A NEW DEVICE FOR FAST AND CONTINUOUS LIQUID-LIQUID EXTRACTIONS ON A MICROLITER SCALE

K. Eberhardt¹, S. Andersson², C. Ekberg², B. Horn³, J.V. Kratz¹,
A. Müller³, M. Nilsson², G. Skarnemark², N. Trautmann¹

¹ Institut für Kernchemie, Universität Mainz, Germany; ² Chalmers University of Technology, Göteborg, Sweden; ³ Institut für Mikrotechnik Mainz, Germany

The fast liquid-liquid extraction system SISAK-3 is based on small centrifuges with continuous feed and output of the liquid phases at flow rates ranging from 0.5 up to 3.0 ml/s [1]. With SISAK-3, the investigation of nuclides with half-lives down to about 1 s is possible. Recently, SISAK-3 combined with an on-line detection system for α -particles and SF-events [2] based on liquid scintillation counting (LSC) has been applied to study 4.3-s ²⁵⁷Rf, produced in the reaction ²⁰⁸Pb(⁵⁰Ti,1n) [3]. From the high flow rates inherent in the application of SISAK-3 various drawbacks result:

- High consumption of organic solvents and extracting agents. Thus, continuous recycling of chemicals during a long-term experiment is irrevocable
- LSC suffers from poor energy resolution and is also sensitive to β -particles and γ -rays interfering with the detection of α -particles.

In order to overcome these problems, a new device for continuous liquid-liquid extraction on a microliter scale has been developed in a co-operation between the Chalmers University of Technology, the Institut für Mikrotechnik Mainz (IMM) and the Institut für Kernchemie. MicroSISAK consists of a stack of microstructured discs with an overall diameter of 8 mm sealed in a Ti-housing. For mixing the aqueous phase with the organic phase, a micro-mixer unit fabricated at IMM is used, where the phases are conducted as two counter-flows through 2 mm long and 20-50 μ m broad interdigital channels (see figure 1a). The laminated flow leaves the device perpendicular to the direction of the feed flows and - due to the small thickness of the lamellae - fast mixing takes place through diffusion [4]. The mixer can be made of titanium, stainless steel or SiO₂. The mixed phases are then fed into a filter unit (see figure 1b) for instant phase separation using a teflon filter with a pore size of 0.5-1 μ m. Here, the aqueous phase is completely retained from the hydrophobous filter, while the organic phase penetrates the filter. A small differential pressure (10-50 mbar) must be applied across the membrane [5]. The volume of the mixer and the filter unit, respectively, is in the order of 2-5 μ l. The system is designed to provide a hold-up time of about 1 s for the mixer-filter combination at a flow rate of 0.02 ml/s. Phase separation has been checked with an aqueous NaCO₃-solution and toluene as organic phase. Aliquots of the

outgoing phases were irradiated at the research reactor TRIGA Mainz. The ²⁴Na-activity in the two phases delivers the phase purity. It could be shown that at flow rates of 0.002-0.04 ml/s less than 0.5% aqueous phase contamination is in the organic phase.

Next, the D-values of Gd extracted into toluene with 2-ethyl-hexyl-orthophosphoric acid (HDEHP) from 0.050 M HNO₃ and of Hf into dibutyl-phosphate (DPB)/toluene from 6 M HNO₃ will be determined. Further experiments are planned to measure the total hold-up time of the system and to optimize the extraction yield for flow rates below 0.002 ml/s. Under these conditions a new detection system can be applied where the outgoing organic phase is evaporated rapidly to dryness and assayed for activity by silicon detectors.

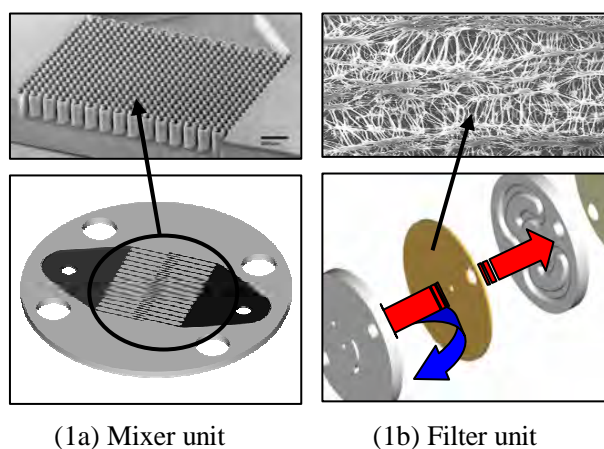


Figure 1: Schematic view of the new MicroSISAK-device with a microstructured unit for intense mixing of phases (1a) and a filter unit for subsequent phase separation (1b).

References

- [1] H. Persson et al., *Radiochim. Acta* **48**, 177 (1989)
- [2] B. Wierczinski et al., *Nucl. Instr. Meth.* **A370**, 532 (1996)
- [3] J.P. Omtvedt et al., *J. Nucl. Radiochem. Sci.* **3**, 143 (2002)
- [4] W. Ehrfeld et al., *Microreactors*, Wiley-VCH Weinheim (2000)
- [5] K. Eberhardt et al., *Institut für Kernchemie Annual Report* (2003)

The search for ^{271}Mt via the reaction $^{238}\text{U} + ^{37}\text{Cl}$

P.M. Zielinski, Ch.E. Düllmann, C.M. Folden III, P.K. Gupta, D.C. Hoffman, H. Mahmud, H. Nitsche, J.M. Schwantes, R. Sudowe (UC Berkeley & LBNL), K.E. Gregorich (LBNL), W.D. Loveland, D. Peterson (Oregon State University), M. Schädel (GSI)

Theoretical calculations show that in the region of the heaviest elements liquid drop fission barriers tend to decrease to zero, and the occurrence of nuclear shells is of special importance for the stability of nuclei [1,2]. Experimentally, the influence of deformed sub-shells at $Z = 108$ and $N = 162$ has been confirmed, with the 20-fold increase in half-life of $^{266}\text{Sg}_{160}$ compared to $^{263}\text{Sg}_{157}$ [3], the 300-fold increase of $^{269}\text{Hs}_{161}$ compared to $^{267}\text{Hs}_{159}$ [4] and the recent discovery of $^{270}\text{Hs}_{162}$ [5]. Production of $^{271}\text{Mt}_{162}$ would allow further examination of the $N = 162$ sub-shell.

Additionally, alpha decay of ^{271}Mt would provide more information on ^{267}Bh and ^{263}Db (alpha and sf) decay properties and, should the half-life of ^{271}Mt exceed 1 second, it might be possible to establish whether Mt behaves as a Group 9 element.

Lighter Mt isotopes were first synthesized in 1982 by Münzenberg et al. [6]. Meitnerium's chemistry has never been studied due to the fact that its two known isotopes (^{266}Mt and ^{268}Mt) have half-lives much less than one second. In order to perform the first chemistry of Mt, a longer-lived isotope needs to be synthesized. Hulet and collaborators attempted such an experiment [7], but could only able to establish a 1 nb cross section upper limit for the reaction $^{254}\text{Es} (^{22}\text{Ne}, 4n) ^{272}\text{Mt}$.

HIVAP [8] predicts a reasonable cross section for the production of ^{271}Mt via the reaction $^{238}\text{U}(^{37}\text{Cl}, 4n)^{271}\text{Mt}$ (Figure 1.). Targets in the form of $^{238}\text{UF}_4$ are available from Oregon State University, the LBNL 88-inch cyclotron staff can provide a stable and intense ^{37}Cl beam, and 95% enriched Na^{37}Cl is commercially available.

During November 2002 & April/May 2003, the Heavy Element Group at LBNL (in collaboration with researchers from Oregon State University and GSI) attempted to synthesize ^{271}Mt at the LBNL 88-inch cyclotron. Reaction products were separated in flight by the Berkeley Gas-filled Separator (BGS) set to cover magnetic rigidities of 2.15-2.35 Tm. A focal plane detector was mounted at the exit of the BGS to measure correlated EVR-alpha, EVR-fission, and alpha-alpha decays. In addition, a multi-wire avalanche counter (MWAC) was mounted upstream of the focal plane detector to give the first TOF signal, and a Si detector was mounted downstream of the focal plane as a punch-through detector. Both the MWAC and the punch-through detectors functioned to veto uninteresting events in the focal plane. A schematic of the setup is shown in Figure 2.

With a total dose of 4.9×10^{18} particles of ^{37}Cl at 195 ± 3 MeV (Center of Target), no events were seen that can be attributed to the production and subsequent decay of ^{271}Mt . A realistic calculation of the upper limit for the one event cross section is 1.5 pb (shown in figure 1). We plan to run further experiments using 5-10 MeV higher projectile energies to examine the 4n & 5n exit channels. Reducing the MWAC thickness from 3.3 to 2.4 microns should increase the EVR implantation energy. We also plan to study the hot fusion cross section systematics using ^{238}U targets.

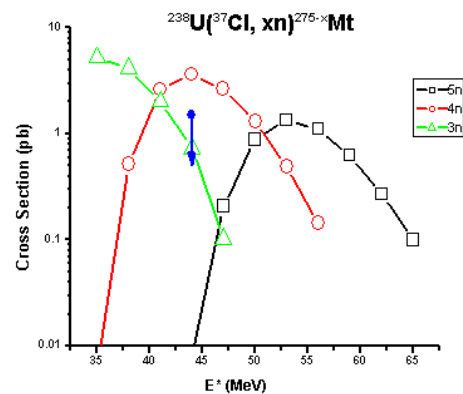


Figure 1. HIVAP prediction (open symbols) with single-event cross section upper limit shown as a solid circle.

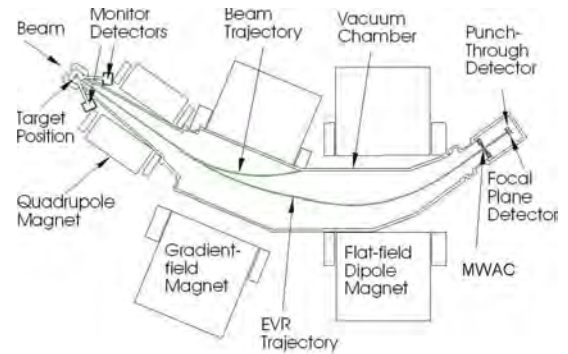


Figure 2. BGS schematic

References

- [1] R. Smolańczuk, Phys. Rev **C56**, 812 (1997)
- [2] S. Hofmann, Rep. Prog. Phys. **61**, 639 (1998)
- [3] R.W. Loughheed, et al., J.Alloy Comp. **213/214**, 61 (1994)
- [4] Yu. A. Lazarev, et al., Phys. Rev. C **54**, 620 (1996).
- [5] A. Türler, et al., Eur Phys J A **17**, 505 (2003)
- [6] G. Münzenberg, et al., Z. Phys. **A309**, 89 (1982).
- [7] E.K. Hulet, Lawrence Livermore National Laboratory E&TR, 17 (1988)
- [8] W. Reisdorf, et al., Z. Phys. **A343**, 47 (1992)

^{20}Ne on ^{244}Pu – first preliminary results

R. Dressler¹, B. Eichler¹, R. Eichler^{1,2}, A. Laube¹, J. Neuhausen¹, D. Piquet¹, H.W. Gäggeler^{1,2},
F. Haenssler², S. Soverna², Qin Zhi², M. Schädel³, E. Schimpf³, K. Eberhardt⁴, P. Thörle⁴,
N. Trautmann⁴

¹PSI, Switzerland; ²University Bern, Switzerland; ³GSI, Germany; ⁴University Mainz, Germany

The isotope ^{259}Rf was firstly investigated in [1] in the 5n channel of the reaction ^{22}Ne on ^{242}Pu . Additionally, the low energy part of the excitation function of ^{256}No , which is produced in the $\alpha 4n$ channel, was reported. Later, only a few experiments have been carried out aiming investigation of nuclear reactions based on Pu and Ne e.g.[2]. We continue our investigation of xn and αxn reactions in the region of Rf and No, which we started already in [3]. The goal is to study the formation and decay properties of ^{259}Rf and ^{256}No produced in the reactions $^{244}\text{Pu}(^{20}\text{Ne}, 5n)$ and $^{244}\text{Pu}(^{20}\text{Ne}, \alpha 4n)$, respectively.

In the course of the experiment a Pu target (enriched 98.6% in ^{244}Pu) with a thickness of 0.55 mg/cm^2 on a Be-backing of 15 mm thickness was irradiated with $^{20}\text{Ne}^{6+}$, at beam energy of 113 MeV in the middle of the target. Typically, the beam intensity was 0.15 - 0.20 pA. Hence, during the 120 h experiment an overall beam dose of $4.7 \cdot 10^{17}$ particles have been accumulated on the target. The recoiling reaction products were transported using a He-KCl-gas-jet (flow rate 1 l/min) to the PSI Tape System within 3 s (estimated transport yield 30%). The aerosols are impacted in vacuum on the tape during 3.8 s and subsequently the samples are moved within 0.4 s in front of 4 consecutive α -PIPS-detectors (450 mm^2 active area, 40% detection efficiency for α -particles). The MIDAS data acquisition system was used for the event-by-event recording [4]. During the entire experiment 17 spontaneous fission (SF) events were detected at an expected background of 1.9. The SF decay data are compiled in Table 1. The sum of the measured α -spectra of detector 2, 3, and 4 are presented in Figure 1. The first detector is omitted, because of the high $^8\text{Be}/^8\text{B}$ background in this detector. The daughter isotopes of ^{259}Rf and ^{256}No (^{255}No and ^{152}Fm , respectively) are too long-lived in order to observe unambiguous time correlated decay chains. kommt jetzt der eigentliche Text.

Table 1: Observed SF energy (E_{SF}) and live time (τ).

Det.No.	E_{SF} [MeV]	τ [s]	Det.No.	E_{SF} [MeV]	τ [s]
1	80.1	3.85	2	70.6	5.60
1	89.4	3.26	2	42.8	5.61
1	99.1	3.38	2	58.0	4.92
1	76.6	0.87	2	54.6	6.45
1	30.9	4.03	2	73.7	5.99
1	30.4	1.26	2	94.4	5.70
1	69.9	1.30			
4	82.3	14.3	4	102.3	16.5
4	58.0	13.4	4	98.6	15.1

Based on the number of measured α - α correlations and single α -events attributed to interfering nuclides, a background in the α -decay energy region of ^{259}Rf and ^{256}No has been estimated (BG). The data are compiled in Table 2.

Unfortunately, this first experiment was not sensitive enough to detect the α -decay of ^{256}No or ^{259}Rf . The origin of the SF-events remains open. Their distribution in all 4 detectors did not allow, a statement about an evident short-lived SF activity attributed to ^{259}Rf . In order to get statistically more significant estimations of interfering long-lived background activities, the number of detectors will be extended up to 8 in future experiments. Furthermore, a daughter mode will be included in order to observe unambiguous α - α -correlations of the ^{259}Rf - ^{255}No ($T_{1/2} = 3.1 \text{ min}$) decays.

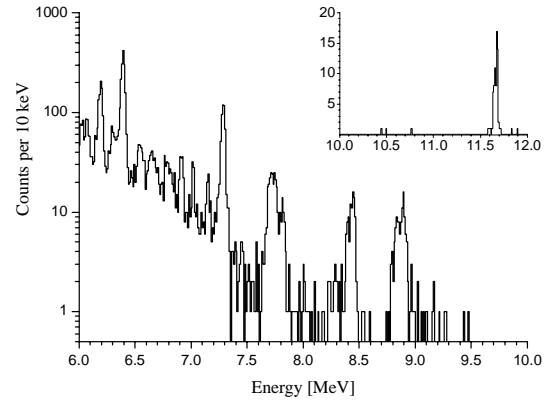


Fig. 1: α -spectra of detector 2, 3, and 4.

Table 2: Observed events in the ^{259}Rf and ^{256}No region, and interfering by-products (BG)

Mother (MeV)	Daughter (MeV)	Events	BG (MeV)
^{221}Ra (6.6–6.8)	^{217}Rn (7.6–7.8)	14	88 (8.4–8.6)
^{221}Ra (6.6–6.8)	^{213}Po (8.2–8.4)	58	145 (8.4–8.6)
^{222}Ac (6.8–7.1)	^{218}Fr (7.4–7.9)	6	15 (8.7–8.9)
^{211}Po (7.2–7.3)		550	60 (8.7–8.9)
^{213}Po (pile up)		28	112 (8.7–8.9)
Mother (MeV)		Events	BG
(^{256}No) (8.4–8.6)		248	233
(^{259}Rf) (8.7–8.9)		184	172

References

- [1] G.N. Flerov, et al., Phys. Lett 13, 73 (1964).
- [2] Yu.A. Lazarev, et al., Phys. Rev. C 62, 064307 (2000).
- [3] R. Dressler, PhD Thesis Uni. Bern (1999).
- [4] R. Dressler, PSI Scientific Report 2002, 68 (2003).

Cross sections measurement in fusion reactions $^{36}\text{Ar}(^{148}\text{Sm}; xn)$

M. Schädel ¹, W. Bröchle ¹, E. Jäger ¹, A. Popeko ², S. Reitmeier ³, E. Schimpf ¹,
R. Sagaidak ², A. Shutov ², A. Türler ³, A. Yakushev ³, A. Yeremin ¹

¹ Gesellschaft für Schwerionenforschung mbH, Darmstadt, Germany

² Flerov Laboratory of Nuclear Reactions JINR, Dubna, Russia

³ Institut für Radiochemie TUM, München, Germany

On the way to neutron-rich superheavy elements (SHE) very exciting results were observed in ^{48}Ca induced reactions with heavy actinide targets[1]. These SHE isotopes have life times several orders of magnitude longer than isotopes produced in “cold fusion” reactions. In the future, reactions with neutron-rich radioactive ion-beams may open a possible path for a further increase of the neutron excess in SHE nuclides. New facilities for radioactive beams are operational or will be constructed. It is of great interest to pursue the “hot-fusion” path and to investigate the projectile-isospin dependence of heavy element fusion-evaporation residue cross sections at Coulomb barrier energies. For this, it is planned to exploit the potential of a facility like SPIRAL which shall provide n-rich radioactive ion beams. Presently, limited beam intensities do not allow to perform systematic studies directly in the region of SHE and heavy actinides with picobarn and nanobarn cross sections, respectively. However, product nuclei with atomic number between 80 and 90 are sufficiently heavy to provide a solid basis for a first study. In addition, for a number of these elements fast and highly efficient chemical separation and detection methods are at hand.

The system ^{18}Ar on ^{62}Sm is a well studied heavy-ion reaction[2]. ^{40}Ar was used as a projectile while target nuclei varied. The wide span of Sm nuclides ranging from ^{144}Sm (on-shell, $\beta_2=0.00$, $T=10$) over ^{148}Sm (off-shell, $\beta_2=0.16$, $T=12$) to ^{154}Sm (off-shell, $\beta_2=0.27$, $T=15$) provided the basis to study, e.g., the effect of static nuclear deformation and of dynamic effects on the fusion cross section. We* opted for this projectile-target-Z combination to extend these studies to probe the neutron excess in radioactive Ar projectiles - up to ^{44}Ar - on the evaporation residue cross section at near barrier energies. While ^{42}Ar and ^{144}Sm have a similar neutron-excess of about 1.32 the N/Z-ratios for the combination ^{36}Ar on ^{148}Sm are 1.00 and 1.39, and for ^{44}Ar on ^{144}Sm they are 1.44 and 1.32, respectively. It is

noteworthy to mention that for the latter system the neutron excess of the projectile exceeds the one of the target. A comparison of results from the spherical, n-rich nuclei ^{44}Ar (off-shell, $N/Z=1.44$) and ^{48}Ca (on-shell, $N/Z=1.40$) can yield information on the influence of shell effects. An important aspect in the evaluation of the results will be the comparison with calculated cross sections. Based on known experimental data such calculations were performed for ^{44}Ar projectiles using a modified HIVAP code[3], see Fig.1.

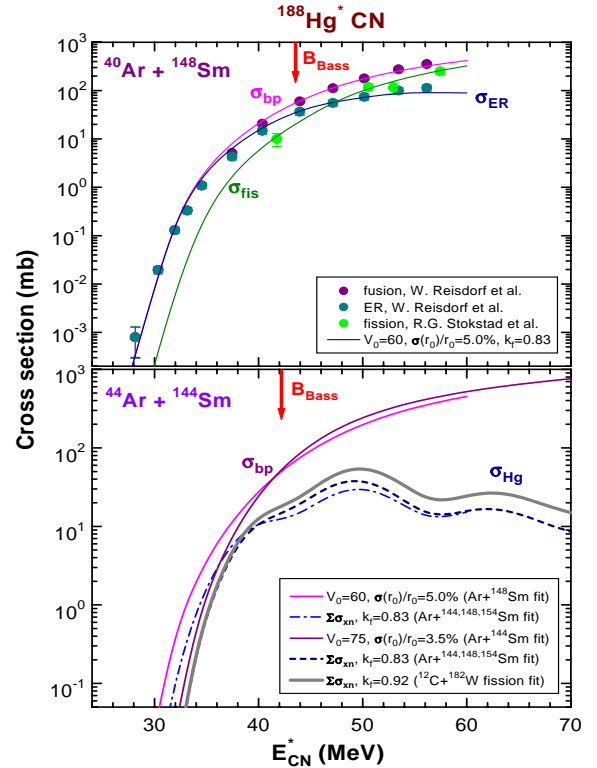


Fig. 1. HIVAP calculations of the $^{44}\text{Ar}+^{144}\text{Sm}$ reaction in comparison with $^{40}\text{Ar}+^{148}\text{Sm}$ reaction.

Most comfortably, Hg, the complete-fusion n-evaporation product in this reaction, is chemically well studied, mainly as the lighter homologue of element 112. Highly efficient

* GSI-Mainz-München-IPN-Orsay-GANIL-FLNR collaboration

separation and detection techniques are at hand to identify individual nuclei[4].

To begin our experimental program aiming finally at using n-rich Ar projectiles we selected the $^{36}\text{Ar}(^{148}\text{Sm}; xn)$ reaction as a first experiment to span a very large range of target-projectile combinations. Ar^{+7} beams from the UNILAC with energies of 7.38 and 7.16 MeV/u, respectively, irradiated a thin ^{148}Sm target ($250 \mu\text{g}/\text{cm}^2$, $\geq 95\%$ ^{148}Sm) on $3 \mu\text{m}$ Ti-backing mounted in X1. Ti foils in thickness of 2, 3, 4, 5, 6, 7, 8 μm served as degraders to reduce the beam energy. Cross sections were measured at energies of 135, 150, 155, 160, 165, 170, 176 and 190 MeV. These energies are uncertain within about 2%. All recoils were thermalized in helium gas and volatile products were transported in the

gas flow ($v=1.84$ l/min) to the detector setup. The detector consisted of 4 pairs of PIPS detectors (2×2 cm) in series. The distance between top and bottom arrays was about 1 mm. The detection efficiency for alpha decay from species adsorbed at the detector surface activity was $\approx 80\%$. Hg isotopes produced as fusion-evaporation residues have a high volatility and were transported to the detector with a high efficiency. The isotopes $^{179,180,181,182}\text{Hg}$ were detected. Cross sections for these isotopes, evaluated from the measured α -spectra, are compared with cross sections theoretically predicted by R. Sagaidak, see Fig 2. Low statistics limited the results for the 2n and 5n channels. The experimental data are typically uncertain by a factor of 2.

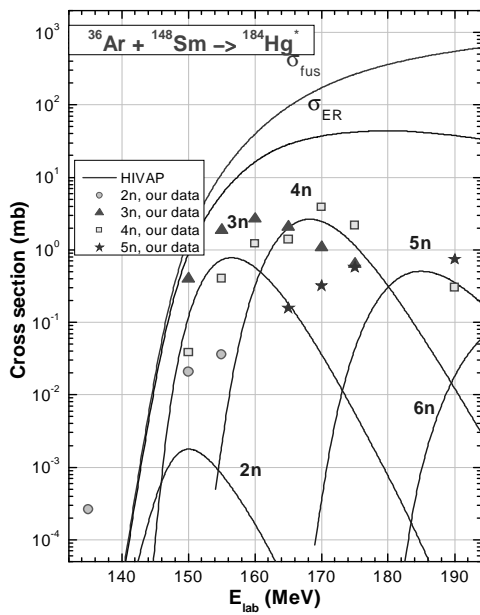


Fig. 2. Measured and calculated cross sections.

-
- [1] Yu. Ts. Oganessian et al. Contribution at TAN'03 Conference, November 16-20, 2003, Napa Valley, USA.
 [2] R.G. Stokstadt et al., *Z. Phys. A* **295** (1980) 269; W. Reisdorf et al., *Phys. Rev. Lett* **49** (1982); W. Reisdorf et al., *Nucl. Phys. A* **438** (1985) 212.
 [3] R. Sagaidak et al. Preprint JINR E7-2003-149, 2003, Dubna, Russia, *Phys. Rev. C* in print.
 [4] A. Yakushev et al. *Radiochim. Acta* **91** (2003) 433.

Towards the 1s Lamb Shift via Crystal Spectrometry

H.F. Beyer¹, Th. Stöhlker¹, D. Banas², D. Liesen¹, D. Protić³, K. Beckert¹, P. Beller¹, J. Bojowald³, F. Bosch¹, W. Brüchele¹, E. Förster⁴, B. Franzke¹, A. Gumberidze¹, S. Hagmann¹, J. Hoszowska⁵, P. Indelicato⁶, O. Klepper¹, H.-J. Kluge¹, B. Kindler¹, St. König⁴, Chr. Kozhuharov¹, B. Lommel¹, X. Ma¹, B. Manil⁷, I. Mohos³, A. Oršić-Muthig¹, F. Nolden¹, U. Popp¹, A. Simionovici⁵, D. Sierpowski², U. Spillmann¹, Z. Stachura², M. Steck¹, S. Tachenov¹, M. Trassinelli⁶, N. Trautmann⁸, A. Warczak², and O. Wehrhan⁴

¹GSI, Planckstraße 1, D-64291 Darmstadt, Germany; ²Institute of Physics, Jagiellonian University, PL-30059 Cracow, Poland; ³FZ Jülich, Institut für Kernphysik, Germany; ⁴Inst. für Optik und Quantenelektronik, F. Schiller-Universität, D-07743 Jena, Germany; ⁵ESRF, F-38043 Grenoble, France; ⁶Lab. Kastler Brossel, Université P. et M. Curie, F-75252 Paris Cdex 05, France; ⁷CIRIL-GANIL, rue Claude Bloche, F-14070 Caen, France; ⁸Institut für Kernchemie, Universität Mainz, D-55128 Mainz, Germany

Since 20 years now quantum-electrodynamics (QED) contributions to the binding energy of high- Z one- and few-electron ions have been studied at GSI. During that period much progress has been made in the way the ions are prepared for experiment, in the theoretical formulation as well as in the accuracy of numerical results for the QED effects and also in the measurement techniques. Lamb-shift experiments of the *first* and *second* generation were confined to use either a high nuclear charge *or* high spectral resolution. In a short test experiment conducted at the ESR in March we proved that a *third-generation* Lamb-shift experiment is now feasible using the high- Z ions *and* high spectral resolution. With this step we anticipate to outperform previous Lamb-shift experiments and to approach the ± 1 eV level of uncertainty which corresponds to the estimated uncertainty of current theoretical QED calculations including two-photon exchange.

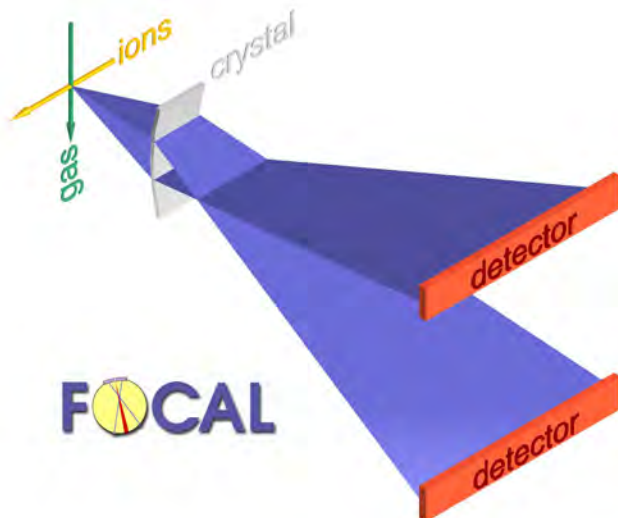


Figure 1: Arrangement of a FOCAL crystal spectrometer.

New crystal optics in the Focusing Compensating Asymmetric Laue (FOCAL) [1] case have been developed along with a high-performance position-sensitive Germanium strip detector [2]. This apparatus has been successfully tested reaching nearly all of its design goals [3]. The experimental arrangement at the ESR gas jet is sketched in figure 1. For the first time the Lyman- α doublet of hydrogen-like Au^{78+} , shown in figure 2, was measured with a crystal spectrometer.

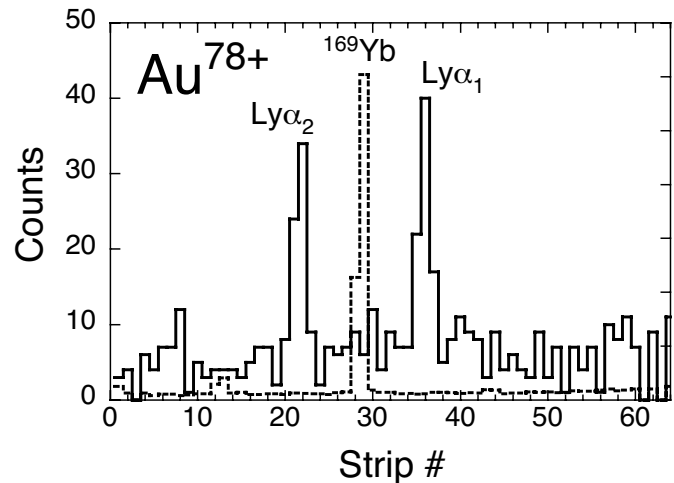


Figure 2: The Lyman- α spectrum of fast hydrogen-like gold measured at the ESR storage ring. For comparison is shown the spectrum from the ^{169}Yb source with the 63 keV gamma-ray line used for calibration.

This experiment has become feasible only with the increased ion numbers stored in the ESR. The other condition is an optimized crystal spectrometer that has an acceptable efficiency and allows for effective background suppression in a low count-rate experiment. The FOCAL x-ray optics have been designed for high systematic wavelength accuracy at an efficiency that is large in comparison with previous crystal-spectrometers for that wavelength range. With this scheme it is possible to measure the line radiation from fast x-ray sources with nearly the same linewidth as for stationary x-ray sources. It also allows blocking of background x rays. In addition we make use of the time and energy resolution of the x-ray detector to set energy and time discrimination in the x-ray-particle coincidences. Although the count rate is low the small background observed is very encouraging for a longer run collecting more statistics.

Supported by a Marie Curie Fellowship of the EC Programme IHP under contract number HPMT-CT-2000-00197.

References

- [1] H. F. Beyer, Nucl. Instrum. Methods. **A400** (1997) 137.
- [2] D. Protić *et al.* IEEE Trans. Instr. Meas. **48** (2001) 1048.
- [3] H.F. Beyer *et al.*, Spectrochimica Acta Part B, *to be published*.